AD-754 949

ON THE DESIGN OF A TOWED ELF H-FIELD
ANTENNA

Michael L. Burrows

Massachusetts Institute of Technology

Prepared for:

Electronic Systems Division

28 December 1972

DOCUMENT CONTROL DATA - R&D

(Security classification of title, body of abstract and indexing annotation must be entered when the overall report is classified)

1. ORIGINATING ACTIVITY *(Corporate author)*	2a. REPORT SECURITY CLASSIFICATION
Lincoln Laboratory, M.I.T.	Unclassified
	2b. GROUP
	None

3. REPORT TITLE

On the Design of a Towed ELF H-Field Antenna

4. DESCRIPTIVE NOTES *(Type of report and inclusive dates)*

Technical Note

5. AUTHOR(S) *(Last name, first name, initial)*

Burrows, Michael L.

6. REPORT DATE	7a. TOTAL NO. OF PAGES	7b. NO. OF REFS
28 December 1972	96	19

8a. CONTRACT OR GRANT NO. F19628-73-C-0002	9a. ORIGINATOR'S REPORT NUMBER(S)
b. PROJECT NO. 1508A	Technical Note 1972-34
c.	9b. OTHER REPORT NO(S) *(Any other numbers that may be assigned this report)*
d.	ESD-TR-72-355

10. AVAILABILITY/LIMITATION NOTICES

Approved for public release; distribution unlimited.

11. SUPPLEMENTARY NOTES	12. SPONSORING MILITARY ACTIVITY
None	Department of the Navy

13. ABSTRACT

The various noise sources known to be troublesome in a towed ELF H-field antenna are examined theoretically and formulas are presented enabling noise voltages to be predicted from other measurable quantities. The treatment identifies the role played by the various contributing factors such as cable vibration, cable properties, core permeability, geomagnetic field, etc., and so indicates the way in which the noises can be reduced. Comparisons with experimentally measured noise voltages support the theory.

14. KEY WORDS

Navy communications	ELF	noise voltages
noise sources	H-field antenna	

MASSACHUSETTS INSTITUTE OF TECHNOLOGY

LINCOLN LABORATORY

ON THE DESIGN OF A TOWED ELF H-FIELD ANTENNA

M. L. BURROWS

Group 61

TECHNICAL NOTE 1972-34

28 DECEMBER 1972

II

LEXINGTON   MASSACHUSETTS

CONTENTS

Appendices

On the Design of a Towed ELF H-Field Antenna

I. Introduction

Over the last few years, the possibility of building an ELF loop antenna (H-field antenna) for towing behind a submarine has been receiving close attention. The principal result of this work is the conclusion that the task can be accomplished only when the many problems are thoroughly understood and then accounted for in the antenna design. Although at present no design of sufficiently good performance exists, much of the basic understanding has been obtained. Thus the work from now on should consist largely of using the understanding as a basis for testing and evaluating candidate construction materials and fabrication methods. To facilitate the work, this report documents that understanding. It does not, however, propose a specific antenna design or predict eventual performance. This cannot be done until after the testing and evaluating stage.

Interest centers on the frequency range of about 20 to 200 Hz in the ELF band because in that range the attenuation in the water and in the earth-ionosphere waveguide is low enough for long-range broadcasting to sub-merged submarines to be feasible [6]. The problem of radiating enough energy from an antenna of practical size is a difficult one, but it appears to be solvable by using a horizontal electric dipole. This kind of antenna can also be used as the receiving antenna on the submarine. Physically it con-

sists of two small electrodes built into a cable and separated by some 200 to 300 m and towed well aft away from the interfering electromagnetic noise field generated by the boat (Fig. 1). It confers on the boat an ability to communicate over a very useful range of depths and speeds. Unfortunately, it is linearly polarized and the downward propagating transmitted signal in the ocean is also mainly or wholly linearly polarized. It suffers, therefore, from the disadvantage that it becomes nearly or wholly blind if the submarine heading is perpendicular to the direction vector of the transmitted electric field. In the far-zone field of the transmitting antenna this occurs when the submarine heading is perpendicular to the great-circle path linking the transmitter and receiver.

The successful development of an H-field antenna built into the same cable would provide a receiving polarization perpendicular to that of the E-field (electrode-pair) antenna. Since the transmitted electric and magnetic fields are mutually perpendicular and essentially horizontal, the H-field antenna, in the form of a long slender solenoidal winding, would be maximally sensitive when the E-field antenna is blind. Communication can therefore be maintained independently of heading (Fig. 2).

The fundamental limitation on ELF communication at the surface is atmospheric noise. Compared with it, the noise generated by the E-field antenna and the interference generated by the boat are both negligibly small.
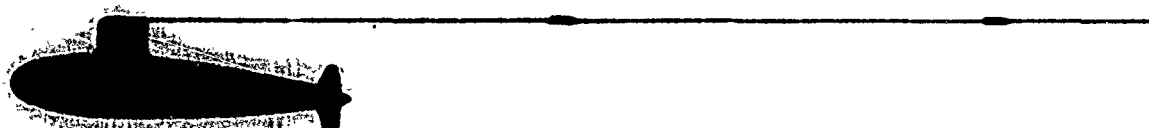
Fig. 1.   Electrode-pair E-field antenna towed from the submarine.

SOLENOID

ELECTRODE

ELECTRODE

$V_h = C_h H \cos \theta$

$V_e = C_e E \sin \theta$

V_h

V_e

E

H

θ
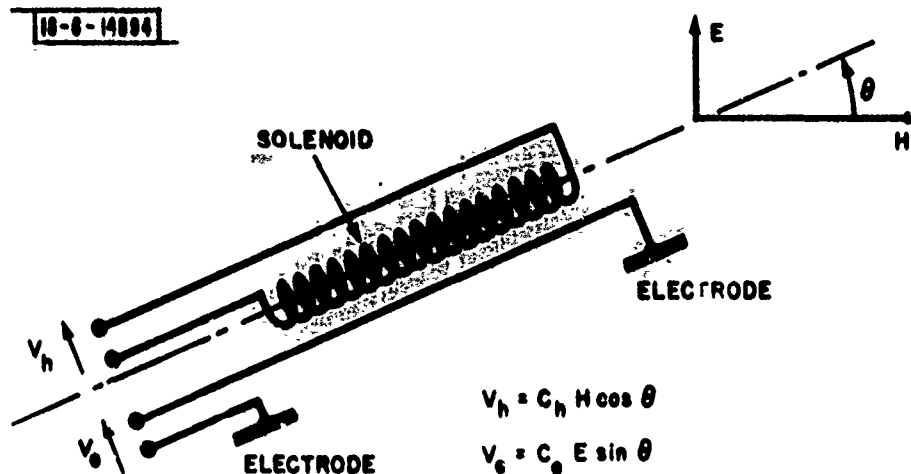
Fig. 2.   Combined E- and H-field antennas for polarization diversity. (C_e and C_h are factors dependent upon the geometrical details of the two antennas.)

3

As the antenna submerges, both signal and atmospheric noise are attenuated by the same amount and so the signal to noise ratio is initially not affected. The communication rate is therefore unimpaired. However, the local noises--from the antenna and the boat--are essentially unaltered by sub-merging. If the antenna depth continues to increase, eventually the atmos-pheric noise level will be equal to that of the local noises, and communica-tion begins to be degraded. Thus the depth of operation is determined by the antenna noise. The design problem, therefore, for the H-field antenna is to reduce the level of the noise it generates to be no greater than that of the E-field antenna.

It is shown in Section III that the thermal noise generated by an H-field antenna without a ferromagnetic core, given the limitations of available conducting materials and the constraint that the antenna cable be positively buoyant, is too high unless the antenna is allowed to become in-conveniently large. One is forced, therefore, to consider using a ferro-magnetic core. Unfortunately, this gives rise to "magnetostrictive" (stress-induced) noise and Barkhausen noise. The former arises because the geomagnetic bias flux density in the core changes its magnitude when the core is stressed by mechanical vibration, thereby inducing a change in voltage in the antenna winding. The latter occurs because the geomagnetic bias flux density in the core does not follow smoothly the changing axial

4

component of the geomagnetic field strength as the boat turns. Rather, it proceeds by a succession of small jumps, which induce voltage transients in the antenna winding. [1, pp. 613 and 524].

Magnetostrictive noise can be reduced by choosing the right core material, by keeping the net bias flux density close to zero by means of an adjustable direct current in the antenna winding [4], by making the antenna long and less sensitive towards the two ends than it is in the middle of its length, by minimizing the stress transmitted to the core and by reducing the level of the cable vibration.

Barkhausen noise can be reduced by choosing the right core material, by keeping the net bias flux density as constant as possible [4] and by increasing the length of the antenna.

Noise is also generated when the geomagnetic flux linking the turns of the antenna winding is modulated by their angular vibration. This is called motion-induced noise and is present whether or not a ferromagnetic core is used. Reducing the cable vibration, making the antenna long, making it less sensitive towards the two ends that it is in the middle of its length and making its variation of sensitivity along its length very smooth are techniques for reducing this noise. A comparison of the motion-induced noise of an H-field antenna, when this is due to ideal cable flexing, with that of an E-field antenna shows that in principle a long H-field antenna need

be no more susceptible to motion-induced noise than the E-field antenna [7].
Recently, however, it has been pointed out that more complicated cable
motion is possible than that due to ideal flexing, but no quantitative esti-
mate is made of the relative magnitude of the resulting noise [19]. Thus
there is as yet no evidence that such motion is an important noise source.
On the other hand, the point is valid in principle and deserves closer
attention.

To date, two long H-field antennas have been made and tested.
Neither is quiet enough to be useful, but their performance taken together
with the improvements likely to be realized by applying the additional tech-
niques covered in this report, suggest that a usefully quiet antenna can be
built. One antenna showed that a low enough thermal noise can be
attained, although it suffered from uncontrolled motion-induced noise due
to independent vibrations of its core elements, while the other antenna
showed that a core construction exists--the helically wound tape core--
which eliminates the offending type of core vibration, although it suffered
from a high thermal noise and a vibration induced noise that appears to be
ascribable to its uniform sensitivity distribution (see Section VII).

The following Sections treat in detail the points mentioned in this
brief summary, except for the newly proposed motion-induced noise mechan-
ism mentioned above which has yet to be fully explored. A brief survey of
the experimental evidence is also included. It gives strong support to those
aspec   theory it touches.

II. Measure of Performance and Effective Length

A convenient measure of antenna quality is one that allows antennas of different configurations and types to be compared and which, at the same time, uses the minimum number of additional assumptions. It should also be some physically identifiable quantity, if possible, to aid in its application.

A measure that fits this prescription well is the ratio of the r. m. s. open-circuit noise voltage to the effective length of the antenna, where the effective length is the length by which an incident electric field must be multiplied to give the corresponding open-circuit antenna voltage. The measure has the dimensions of volts per meter and is physically the horizontal electric field, evaluated at the depth of the antenna, which produces an antenna voltage equal to the noise. In general, the ocean conductivity and, for antennas with an appreciable vertical dimension, a depth reference point on the antenna must be specified. No assumptions about the strength of the transmitted field or of the atmospheric noise field are required. Neither is it necessary to specify any particular depth of operation.

The term "equivalent noise field" or ENF will be used to denote this measure of performance.

For the trailing E-field (electrode-pair) antenna, the effective

length is simply the distance between the electrodes. Thus the total ENF for this antenna is its measured noise voltage divided by the electrode separation. Typical ENF spectra at 8 and 14 knots are shown in Fig. 3 for a 300-meter electrode-pair antenna [3]. For this length of antenna, the noise is now believed to be dominated by motion-induced noise. Under the conditions 14 knots and 45 Hz (to be adopted here as the standard), Fig. 3 shows the ENF of the 300 meter E-field antenna to be -205 dBE.

For a horizontal H-field antenna immersed in the ocean, the effective length can be calculated using Faraday's law. If H is the axial component of the incident magnetic field, then the induced voltage per meter length of antenna is given by $\omega\mu_c HAN$, where ω is the radian frequency, μ_c the reversible permeability of the antenna core, A the cross-sectional area of the core and N the turns density (turns per meter) in the antenna winding. The total antenna voltage V is given therefore by

$$V = \omega H \int \mu_c A N dz = \ell_e E \qquad (1)$$

where the integral is carried out over the complete antenna length, and E is the incident electric field associated with the magnetic field.

Both signal and atmospheric noise propagate down into the ocean from the surface. At ELF, the field components E and H are essentially horizontal and mutually orthogonal. They are related by the wave impedance of the ocean, $\sqrt{-i\omega\mu_o/\sigma}$, σ being the conductivity of the water and μ_o the permeability of free space. Using this relation in (1), one obtains,
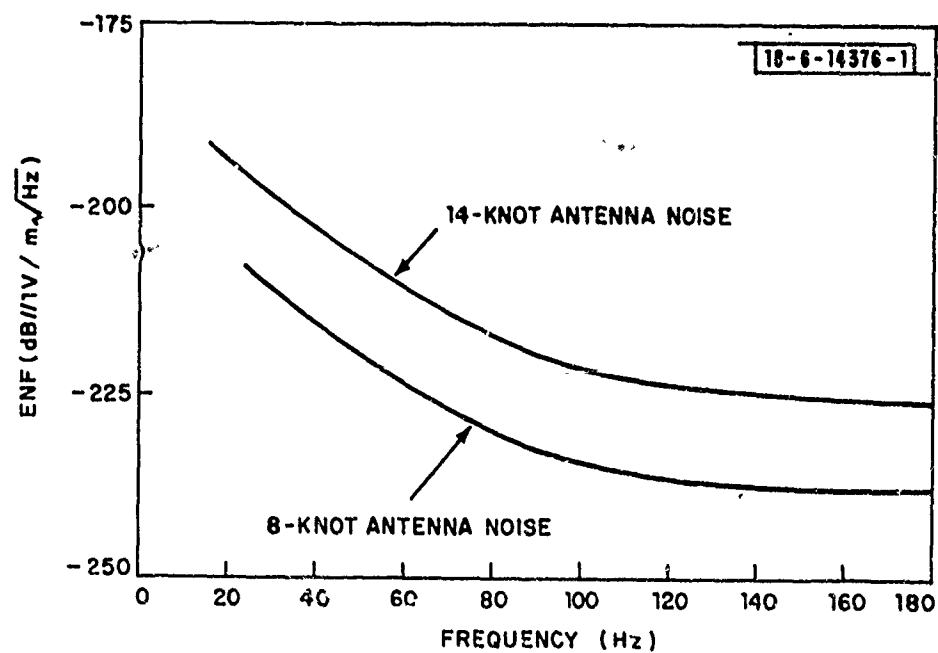
Fig. 3.   Typical equivalent noise field spectra for a 300-meter trailed
E-field antenna at two towing speeds.   (From Griffiths [3].)

in magnitude

$$\ell_e = \frac{\sqrt{2}}{\delta} \int \mu_a A N \, dz \tag{2}$$

where $\mu_a = \mu_c/\mu_o$ is the relative small-signal permeability of the core and δ, defined as $\sqrt{2/(\omega \sigma \mu_o)}$, is the skin depth for electromagnetic propagation into the ocean.

This formula has been obtained by neglecting the magnetic flux in the area occupied by the antenna winding. This flux density links the outer layers of the antenna winding. The permeability of this part of the cross section is that of free space, however. Thus (2) is valid provided the addition of the core increases the antenna inductance by a large factor.

The effective length of an H-field antenna can be accurately estimated by measuring its impedance in air or in the ocean. Appendix A shows that its impedance in the ocean is negligibly different from its impedance in air, and the inductance L_o in air is given simply by

$$L_o = \mu_o \int \mu_a A N^2 \, dz . \tag{3}$$

Thus, if the turns density is uniform, (2) and (3) can be combined to give

$$\ell_e = \frac{\sqrt{2} \, L_o}{\delta \mu_o N} . \tag{4}$$

If the turns density is not uniform, but the *product* $\mu_c A$ is, then (2) and (3) yield

$$\ell_e = \frac{\sqrt{2} \, L_o}{\delta \mu_o} \frac{\int N \, dz}{\int N^2 \, dz} , \tag{5}$$

in which the ratio of integrals can be evaluated from the winding specification of the antenna.

III. Thermal Noise

The thermal noise of the antenna is the noise generated by the resistance of the antenna measured at the antenna terminals. This resistance is the sum of the resistance of the connecting wires, the resistance of the antenna winding and the "radiation" resistance of the winding, which represents the losses in the antenna core and in the surrounding ocean. The core losses can be calculated using standard methods [2, p. 78 ff.] and can, in any case, be avoided by subdividing the core to interrupt the induced circulating currents. The losses in the water are difficult to calculate in general but Appendix A shows that their contribution to the ENF is very small. The resistance of the connecting wires can be made small compared with that of the winding by using a large enough number of turns on the antenna winding. Thus the critical component of the thermal noise is that contributed by the antenna winding.

It is instructive to examine first what can be achieved without a ferromagnetic core in the antenna. In Appendix B, it is shown that even if all the weight of the cable were devoted to the winding and if insulation, where necessary, could be infinitesimally thin, then the minimum thermal ENF attainable in a 300 m length of the current 0.65 in. O.D. buoyant antenna cable at 45 Hz is about -180 dBE. This could be reduced to the required -205 dBE by increasing the diameter by a factor of about 4 or increasing the length by a factor of about 300. The latter is certainly impracticable; the former, since it implies an increase of volume by a factor of sixteen, is still excessive. A ferromagnetic core, therefore, would seem to be essential.

Since the reversible permeabilities attained by currently available ferromagnetic materials can be several tens of thousands times larger than that of free space, the effective length of the antenna can be increased enormously, without any increase in the thermal noise. Thus the thermal ENF can be reduced substantially. The difficulties are that i) a long, slender, high permeability core may be magnetically saturated by the geomagnetic field and thereby lose, temporarily, its high reversible permeability, ii) the stretching and flexing of the cable may plastically strain the core material, causing a permanent loss of its high reversible permeability, iii) the longitudinal cable vibrations, transmitted to the core, generate magnetostrictive (i.e., strain-induced) noise, and iv) the variations of the axial geomagnetic field component due to heading changes can generate Barkhausen noise.

Geomagnetic core saturation can be prevented by using a core material of relatively low permeability or by driving a direct current of the appropriate magnitude and sense through the antenna winding to bring the net flux density in the core close to zero. This latter technique can be made automatic by using an out-of-band sensing signal to monitor continuously the inductance of the antenna and make appropriate changes in the bias current [4].

The plastic strain problem must be dealt with by careful mechanical design, and techniques for reducing magnetostrictive noise and Barkhausen noise are discussed in later sections.

The addition of a ferromagnetic core raises the question of

12

determining the optimum proportions of winding and core. The buoyancy restriction places a limit on the total (reduced) weight per unit length of the core plus winding. Thus the minimum thermal ENF is achieved at a proportion somewhere between the all-conductor one, with its low effective length and the all-core one, with its very high resistance.

If a is the core radius, b the outer winding radius, 2ℓ the antenna length and σ_w the wire conductivity, then assuming that μ_a, the average relative permeability of the core, is large compared with unity, the effective length of the antenna is *

$$\ell_e = 2\pi a^2 \mu_a \sqrt{2} \, N\ell/\delta \tag{6}$$

while the total winding resistance is

$$R = \frac{2\pi N^2 \ell}{\sigma_w} \frac{b+a}{b-a} \quad , \tag{7}$$

assuming in each case that the turns density N, the permeability, μ_a, and the geometry are independent of length. Thus, from (6) and (7), the power spectral density $S_e(\omega)$ of the thermal ENF is given by

$$S_e(\omega) = \frac{k_b T_k \ell^2}{\pi \sigma_w \mu_a^2 \, \ell} \frac{b+a}{a^4(b-a)} \tag{8}$$

where k_b is Boltzmann's constant and T_k the absolute temperature (°K).

On the other hand, the reduced mass per unit length w' of the antenna is given by

$$w' = \pi a^2 \rho_c' + \pi(b^2 - a^2)\rho_w' \tag{9}$$

where ρ_c' is $\rho_c - \rho_b$, and ρ_w' is $\rho_w - \rho_b$. The densities ρ_c, ρ_w and ρ_b are those of the core, the winding and the buoyant flotation material (foamed

polyethylene in the current buoyant antenna cable). The reduced densities ρ_c' and ρ_w' appear in (9) because the antenna core and winding displace not free space or air but the buoyant flotation material.

The problem, then, is to minimize (8) while keeping (9) fixed at the maximum allowed by the buoyancy restriction. This is easily done, for at this optimum state, the total differential of (8) and of (9) must both be zero. That is

$$dS_e(\omega) \equiv 0 = \frac{2 k_b T_k \delta^2}{\pi \sigma_w \mu_a^2 \ell} \cdot \frac{1}{a^5 (b-a)^2} [(2a^2 + ab - 2b^2)da - a^2 db]$$

$$dw' \equiv 0 = 2\pi [(\rho_c' - \rho_w') a\, da + \rho_w' b\, db] .$$

For these equations to have a solution, the determinant of their coefficient matrix must be zero. That is

$$(2a^2 + ab - ab^2) \rho_w' b + a^3 (\rho_c' - \rho_w') = 0$$

or, with $\beta = \rho_c'/\rho_w' = (\rho_c - \rho_b)/(\rho_w - \rho_b)$ and $\alpha = b/a$,

$$2\alpha^3 - \alpha^2 - 2\alpha - \beta + 1 = 0. \tag{10}$$

The functional relationship between α and β is presented graphically in Fig. 4.

Thus, given the densities ρ_c, ρ_w and ρ_b, one calculates β and then solves (10) (or uses Fig. 4) to evaluate the optimum radius ratio b/a. From this, the individual radii a and b can be found by using (9) and these then substituted in (8) to give the minimum value of the thermal ENF power spectrum.
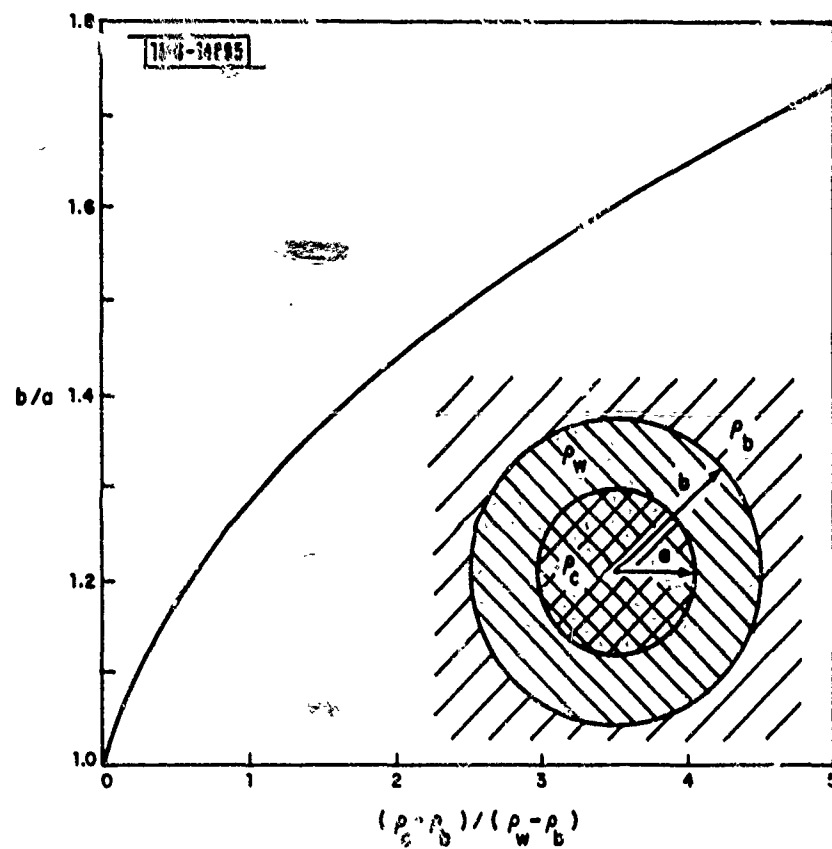
14

Fig. 4. Optimum ratio α of outer to inner winding radii as a function of $\beta = (\rho_c - \rho_b)/(\rho_w - \rho_b)$.

It is not necessary in practice to achieve precisely the optimum proportions, because large deviations from the optimum cause relatively minor degradation in the thermal ENF. To demonstrate this, one notes that if w' and ρ_w' are given, then (9) shows that $1/a^2$ is proportional to $\beta + \alpha^2 - 1$, which means, from (8), that the mean square thermal ENF is proportional to $(\beta + \alpha^2 - 1)^2 (\alpha + 1)/(\alpha - 1)$. This function is plotted, with α (equal to b/a) as the abscissa, for various values of β in Fig. 5. The curves show that the relative winding thickness $\alpha - 1$ can vary over a range of at least three to one without increasing the minimum thermal ENF by more than 1 dB.

The total reduced mass per unit length that the cable can support is given simply by $\pi c^2 (\rho - \rho_b)$, where c is the outside cable radius and ρ is the average density required for the complete cable. However, some of this (say, w_a') may have to be allocated to strength members or some other essential piece of the structure. Thus the available reduced mass per length w' to be allocated to the antenna is $\pi c^2 (\rho - \rho_b) - w_a'$.

In the current buoyant antenna cable, for example, c is 0.325 inches, ρ_b is $0.63\rho_o$ and the 18 fiberglass strength members are each 0.038 inches in diameter and have a density of about $1.67\rho_o$. (Here ρ_o is 10^3 kg/m^3, the mass density of water). Thus w_a' is $18 \times (0.019 \times 0.0254)^2 \times \pi \times (1.67 - 0.63)$ and so, if ρ is to be $0.85\rho_o$, then $w' = 0.0334$ kg/m.

But, if the core density ρ_c is $8.5\rho_o$ and the winding density ρ_w is 2.7, then $\beta = 3.802$ and, from (10), $b/a = 1.636$. Using (9), one then finds that $a = 0.968 \times 10^{-3}$ m. Finally, taking δ to be 37.5m, k_b to be
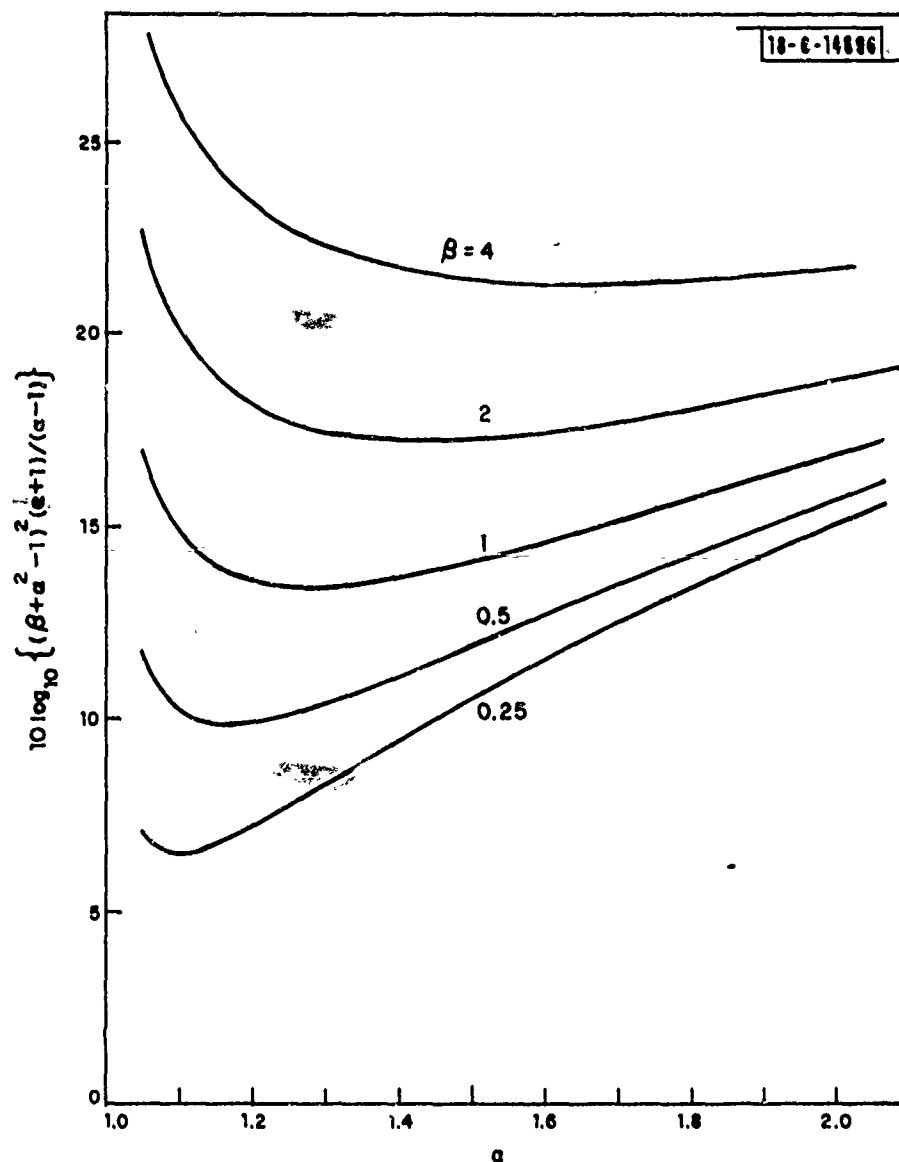
Fig. 5. Relative thermal ENF as a function of the "proportion parameter" α, the net cable buoyancy being held constant.

1.38×10^{-23} J/°K, T_k to be 300°K, σ_w to be 3.57×10^7 mho/m and 2ℓ to be 300 m, one finds that *in order* for the thermal ENF to be -205 dBE, the relative core permeability must be 746.

In practice, the cross-sectional area of the ferromagnetic part of the core will be some fraction γ of the total core cross section. If the remaining space is filled with a material having the density ρ_n, then the average density of this composite core is given by $\rho_c = \gamma \tilde{\rho}_c + (1 - \gamma)\rho_n$ and its average relative permeability is given by $\mu_a = \gamma \mu_r$, where $\tilde{\rho}_c$ and μ_r are the density and relative *permeability* of the ferromagnetic component of the composite core. Table I shows the result of calculating the relative permeability required for the thermal ENF to be -205 dBE for a range of values of the core utilization factor γ. The assumptions are that $\tilde{\rho}_c = 8.5\rho_o$ and $\rho_n = \rho_o$. The core diameter is a function of γ because ρ_c depends on γ and hence the optimum proportions vary with γ.

Required μ_r for the Thermal ENF to be -205 dBE

γ	Core O. D. (inch)	b/a	μ_r
.005	0.291	1.0814	24794
.01	0.280	1.0877	13000
.02	0.260	1.0998	7073
.05	0.220	1.1333	3450
.1	0.182	1.1820	2174
.2	0.144	1.2622	1471
.5	0.101	1.4364	966
1. 0	0.076	1.6355	746

Table I

18

The relative permeabilities specified in Table I apply to an antenna having a uniform sensitivity profile. A more likely profile is one that is parabolic, because it discriminates better against vibration noise (both magnetostrictive and motion-induced). In this case, the permeability would have to be raised by the factor $3/2$ to maintain the same antenna effective length. And, if the ferromagnetic material is applied in the form of a helix of helix angle θ, then the permeability must be increased by the further factor $1/\cos^2\theta$.

It should be noted that the numbers appearing in Table I are the result of a particular set of assumptions. Changing the assumptions can cause a large change in the required permeability. For example, if ρ (the average mass density of the complete antenna cable) is taken to be ρ_o instead of $0.85\,\rho_o$, then w' is nearly twice as large, which means that the required permeabilities are only one quarter of the values shown.

The permeabilities shown in Table I are mostly small compared with the high permeabilities attained by modern ferromagnetic alloys. The mechanical constraints imposed by this application are severe, however. They make it impossible to realize even a small fraction of this potential. As a last resort, the cable diameter could be increased, for, as (8) shows, if all transverse dimensions are doubled, the required permeability is reduced by a factor of four.

IV. Motion - Induced Noise

If $v(z, t)$ is the transverse displacement of the antenna center line, as a function of time and of position along the antenna, from its

19

nominally straight condition, then $\partial y / \partial z$ is the tangent of the angle it makes with the z axis. Provided $|\partial y / \partial z| \ll 1$, therefore, the geomagnetic flux linkage per unit length is given by $A(z)N(z)(B_z + B_y \, \partial y / \partial z)$, where $A(z)$ is the area of the antenna winding, assumed for the moment to have an air core, and $N(z)$ is its turns density (turns per meter). The geomagnetic *field* is assumed to lie in the yz plane, so only its two components B_y and B_z appear.

The total motion-induced voltage $v(t)$ is given by the integral over the length of the antenna of the time rate of change of the flux linkage per unit length. Thus, since $\partial B_z / \partial t = \partial B_y / \partial t = 0$,

$$v(t) = B_y \int A(z)N(z) \, \frac{\partial^2 y(z,t)}{\partial z \, \partial t} \, dz. \tag{11}$$

In Appendix C it is shown that the same equation applies if the antenna has a ferromagnetic core, except that $A(z)N(z)$ must include the additional factor μ_a, the relative incremental permeability averaged over the core area.

This expression can be simplified in the case of the uniform solenoidal winding, for then $A(z)N(z)$ is a constant, say $A_o N_o$, over the length of the antenna, and is zero elsewhere. The expression then reduces to

$$v(t) = B_y A_o N_o \, \frac{\partial}{\partial t} \, \{y(\ell, t) - y(-\ell, t)\} , \tag{12}$$

assuming that the antenna extends from $-\ell$ to $+\ell$ along the z axis. Thus only the vibration of the two end-points generates the noise voltage, no matter how long the antenna is. By simply preventing the ends from vibrating, one can reduce the noise voltage to zero even though the rest of the antenna

vibrates in a completely arbitrary way.

It is impractical to prevent a particular point on the towed cable from vibrating, but this uniform-winding example immediately suggests another way of reducing the motion-induced noise voltage. For the noise voltage is clearly associated with the discontinuities at $\pm \ell$ of the "sensitivity profile" $A(z)N(z)$. Where the profile is uniform, no noise is generated. Thus a profile which is as uniform as possible (within the constraint that it must be zero for $|z| > \ell$) should generate the least noise.

One cannot simply remove the discontinuities at the ends of a uniform profile. For then, being zero at $\pm \ell$, the profile must be zero everywhere and the antenna no longer exists. One seeks therefore a non-uniform profile which goes to zero at $\pm \ell$. For this class of function, an integration by parts converts (11) to the form

$$v(t) = -B_y \int u'(z) \frac{\partial y(z, t)}{\partial t} \, dz , \qquad (13)$$

where the more compact notation $u(z)$ has been used for the sensitivity profile $A(z)N(z)$ and $u'(z)$ stands for $du(z)/dz$.

It appears that in the frequency band of interest here, the sources of the transverse cable vibrations are the stress fluctuations at the cable surface due to the turbulent fluid flow past the obstacle presented by the cable itself (see Appendix D), and the large attenuation for transverse mechanical waves along the cable (see Appendix I) isolates the antenna from disturbances generated by the ship. Thus the motion-induced noise arises from a statistically uniform distribution of transverse forces which are essentially

uncorrelated from point to point along the cable. And since they are uncor-
related, the total voltage is equal to the square root of the sum of the
squares of the voltages generated by each elemental force separately.

To calculate the separate voltages it is more convenient to work
in the frequency domain, in which (13) can be expressed as

$$V(\omega) = i\omega B_y \int u'(z) Y(z, \omega) dz , \qquad (14)$$

where V and Y are the Fourier transforms of v and y. But in this notation,
the displacement $Y(z, \omega)$ caused by a single transverse force $F(\omega)$ applied
at the point z_o is given by $G(z, z_o, \omega) F(\omega)$, where $G(z, z_o, \omega)$ is the Green's
function, and is the displacement at z due to a unit force of radian frequency
ω applied at z_o. Hence the voltage induced by this force is, from (14),

$$V(\omega) = i\omega B_y \int u'(z) G(z, z_o, \omega) dz \, F(\omega) . \qquad (15)$$

The power spectral density $\hat{S}_v(\omega)$ of the antenna voltage induced by this
single force is, therefore, from (15), given by

$$\hat{S}_v(\omega) = \omega^2 B_y^2 \hat{S}_f(\omega) \left| \int u'(z) G(z, z_o, \omega) dz \right|^2 \qquad (16)$$

where $\hat{S}_f(\omega)$ is the power spectral density of the force. Thus, if there is
a uniform distribution of M of these forces per unit length, each one statis-
tically independent of the others, then the total power spectral density
$S_v(\omega)$ of the antenna voltage is

$$S_v(\omega) = \omega^2 B_y^2 M\hat{S}_f(\omega) \int \left| \int u'(z) G(z, z_o, \omega) dz \right|^2 dz_o . \qquad (17)$$

Now $M\hat{S}_f(\omega)$ is related to $S_f(k, \omega)$, the two-dimensional power
spectral density of the transverse force distribution on the cable, defined as

22

$$S_f(k, \omega) = \int C_f(\zeta, \tau) e^{-ik\zeta + i\omega\tau} d\zeta\, d\tau \qquad (18)$$

where $C_f(\zeta, \tau)$, the two-dimensional correlation function, is the expected value of $f(z, t) f(z+\zeta, t+\tau)$ and $f(z, t)$ is the transverse force per unit length. Since the mean square total force on a piece of cable which is long compared with the correlation length of the force distribution is $S_f(0, \omega)$ times the length, on the one hand, and $M\hat{S}_f(\omega)$ times the length, on the other, then the relationship is simply $M\hat{S}_f(\omega) = S_f(0, \omega)$.

The antenna voltage power spectrum can therefore be rewritten as

$$S_v(\omega) = \omega^2 B_y^2 S_f(0, \omega) \int \left| \int u'(z) G(z, z_o, \omega) dz \right|^2 dz_o . \qquad (19)$$

Further analysis is complicated by the fact that the tension in a towed cable increases linearly from the free end towards the tow point. This, in turn, means that the mechanical dynamics of the cable are non-uniform, and so, in particular, that $G(z, z_o, \omega)$ depends upon the sum of the pair z, z_o in addition to their difference. One fundamental result can be obtained fairly simply, however, on the assumption that the sensitivity profile $u(z)$ is both perfectly parabolic and also very long compared to the linear extent of the region of influence of a force applied at a point [i.e., long compared with the "width" of $G(z, z_o, \omega)$]. If these conditions are met, the $u'(z)$ is essentially a constant over the "width" of $G(z, z_o, \omega)$ and so can be taken outside the inner integral and assigned the value $u'(z_o)$. But then $\int G(z, z_o, \omega) dz$, assuming that the tension is essentially invariant over the "width" of $G(z, z_o, \omega)$, can be calculated by assuming the tension

is constant at the value it takes at z_o. Appendix E shows that the integral is then given by $-1/(\omega^2 m_t)$, where m_t is the effective *transverse* vibrating mass per unit length of cable. Thus, for $u(z)$ sufficiently long and sufficiently smooth, (19) can be rewritten as

$$S_v(\omega) = \frac{B_y^2}{\omega^2 |m_t|^2} S_f(0, \omega) \int |u'(z_o)|^2 dz_o \qquad (20)$$

The motion-induced ENF power spectrum $S_e(\omega)$ is given, therefore, by dividing (20) by the effective length squared. Therefore, from (2) and (20), and using the relation $u(z) = \mu_a(z) A(z) N(z)$, one finds

$$S_e(\omega) = \frac{B_y^2 \delta^2}{2\omega^2 |m_t|^2} S_f(0, \omega) \frac{\int |u'(z)|^2 dz}{\left[\int u(z) dz\right]^2} \qquad (21)$$

For a given cable size, cable buoyancy, measuring frequency and towing speed, all quantities in the right member of (21) are predetermined except for $u(z)$. Thus the problem is to choose $u(z)$ to minimize the quotient of integrals appearing in (21) with the constraint that $u(z)$ is continuous for all z and zero for $|z| \geq \ell$. By *applying* the calculus of variations one finds the solution to be

$$u_o(z) = \begin{cases} u_o(0)[1 - (z/\ell)^2], & |z| < \ell \\ 0, & |z| \geq \ell \end{cases} \qquad (22)$$

and this will be referred to as the "parabolic sensitivity profile" on account of its shape, shown in Fig. 6. For this optimum profile, the quotient of
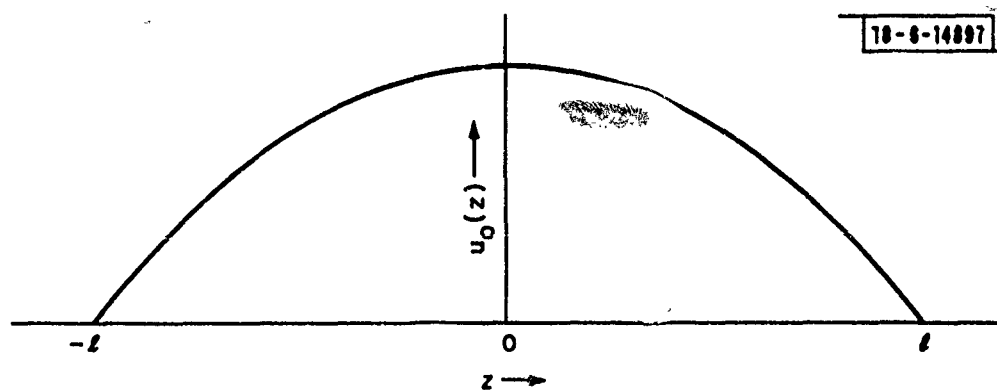
Fig. 6. Optimum sensitivity profile (parabolic profile) for minimizing the motion-induced ENF.

integrals reduces to the expression $3/(2\ell^3)$, and so

$$S_e(\omega) = \frac{3}{4\ell^3} \left(\frac{\delta B_y}{\omega |m_t|} \right)^2 S_f(0, \omega) . \tag{23}$$

Significant features of this formula are, first, that the tension, bending stiffness and energy absorption of the cable do not appear in it, only the transverse force spectrum and the effective mass. Thus since the buoyancy is essentially predetermined, the motion-induced ENF at a particular speed and frequency depends only upon cable diameter and antenna length (provided the "long, smooth profile" assumption is not violated).

Also of interest is the fact that the absolute antenna sensitivity does not appear in the formula. This means that the motion-induced ENF depends only upon the shape of the sensitivity profile and not upon whether or not a ferromagnetic core is used, for example.

In Appendix G, it is shown that the motion-induced ENF of an E-field antenna (the electrode-pair antenna) is given by $B_y^2 S_f(0, \omega)/(2\ell\omega^2 |m_t|^2)$. Comparing this expression with (23), one sees that if the two antennas are of equal length, then they generate the same motion-induced ENF when they are $\sqrt{6} \delta$ long. When they are shorter than this, the H-field antenna is noisier than the E-field antenna, and when they are longer than this, the reverse is true. In a 4 mho/m ocean at 45 Hz, δ is 37.5 m. Thus $\sqrt{6} \delta$ is 91.8 m or about 300 feet. (This comparison depends upon the additional reasonable assumption that $S_f(0, \omega)$ is the same for both the x- and the y-directed transverse force distribution. That is, that the transverse

buffeting forces are statistically azimuthally uniform).

A more difficult question to treat is the modification of (23) required to take into account the effect of a short, rough sensitivity profile. This will be carried out under the assumption that the tension is constant over the whole length of the antenna. The further slight modification required to account for varying tension is examined in Appendix H.

The basic motion-induced noise equation is (19) in which, since now the tension is being assumed constant, $G(z, z_o, \omega)$ can be written as $G_o(z - z_o, \omega)$. Then, with the definitions

$$U(k) = \int u(z) e^{-ikz} dz$$

$$u(z) = \frac{1}{2\pi} \int U(k) e^{ikz} dk$$

(24)

$$H_t(k, \omega) = \int G_o(z, \omega) e^{-ikz} dz$$

$$G_o(z, \omega) = \frac{1}{2\pi} \int H(k, \omega) e^{ikz} dk ,$$

the integral $\int u'(z) G_o(z - z_o, \omega) dz$ can be rewritten as $i(2\pi)^{-1} \int k U(k) H_t(k, \omega) \exp(ikz_o) dk$ and so (19) reduces to

$$S_v(\omega) = \omega^2 B_y^2 S_f(0, \omega) \frac{1}{2\pi} \int k^2 |U(k)|^2 |H_t(k, \omega)|^2 dk . \quad (25)$$

If the assumption that the transverse buffeting forces are essentially uncorrelated from point-to-point along the cable is not valid, then it follows that $S_f(0, \omega)$ in (25) must be included under the integral sign as $S_f(k, \omega)$. Thus the "uncorrelated forces" assumption is equivalent to making the assumption that the spatial spectrum of the force distribution is white

(uniform) over the range of k for which the product $|kU(k)H_t(k,\omega)|^2$ has non-negligible magnitude. In Appendix D, this assumption is shown to be satisfied in practice.

The functions $|U(k)|^2$ and $|H_t(k,\omega)|^2$ appearing in the integrand in (25) are sketched in Fig. 7. The peak in $|U(k)|^2$ reflects the fact that to receive the signal, the winding must be unidirectional, so that u(z) has a large "d. c." component at k=0. The peaks of $|H_t(k,\omega)|^2$ occur at $k = \pm k_t$, where k_t is the real part of the ordinary characteristic wave number for transverse wave propagation at radian frequency ω along the cable. (Since the cable is not perfectly flexible, there also exists an "extraordinary" characteristic wave number. It has a large imaginary part, however, and so does not have a readily visible effect on the shape of $|H_t(k,\omega)|^2$ along the real k axis.)

If the sensitivity profile u(z) is very long and very smooth, then its Fourier transform U(k) will be very peaked at the origin and be very small elsewhere. Then the integrand in (25) (the product with k of the two functions sketched in Fig. 7), will be of negligible magnitude for all k except for two narrow regions symmetrically placed either side of and close to the point k=0. But over these regions, $|H_t(k,\omega)|^2$ is essentially equal to $|H_t(0,\omega)|^2$ and so the integral in (25) can be rewritten as $|H_t(0,\omega)|^2 \int |kU(k)|^2 \, dk$, which, by virtue of Parseval's theorem, can be re-expressed as $2\pi |H_t(0,\omega)|^2 \int [u'(z)]^2 \, dz$. Substituting this back in (25), and noting, from Appendix E, that $H_t(0,\omega) = -1/(\omega^2 m_t)$, one finds that (25) reduces to (20). Thus the contribution of the peak in $|U(k)|^2$ at the origin to

$|U(k)|^2$

$|H_t(k,\omega)|^2$
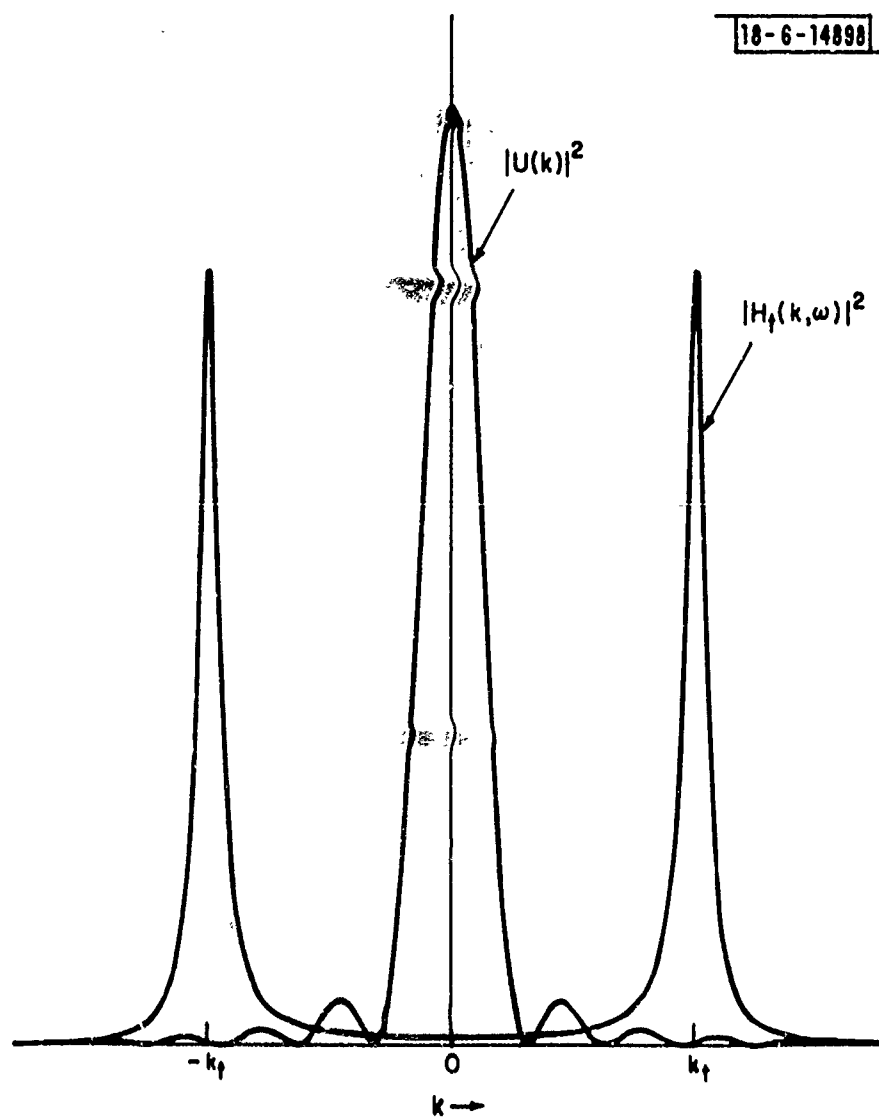
$-k_t$ 0 k_t

$k \longrightarrow$

Fig. 7. Sketch of $|U(k)|^2$ and $|H_t(k,\omega)|^2$.

the integral in (25) is simply the fundamental long, smooth profile contribution discussed earlier.

There are two other peaks in the integrand in (25), however, whose contribution must also be included. If the profile $u(z)$ is short enough, but still smooth, then the minor peaks of U(k) will make the contribution of the integrand arising from the peaks of $H_t(k, \omega)$ at $k = \pm k_t$ larger than that arising from the peak in U(k) at k=0. Since the peaks of $H_t(k, \omega)$ are in practice very high and sharp, their contribution to the integral in (25) can be written $k_t^2 \mathrm{Av}\{|U(k_t)|^2\} \int |H_t(k, \omega)|^2 dk$, where $\mathrm{Av}\{|U(k_t)|^2\}$ is a local average of $|U(k)|^2$ centered on the points $\pm k_t$. But, from Appendix E, $\int |H_t(k, \omega)|^2 dk$ is the same as $2\pi S_y(\omega)/S_f(0, \omega)$, where $S_y(\omega)$ is the spectral density at frequency ω of the transverse displacement of the antenna at a point.

Thus (25) can be expressed in the approximate form

$$S_v(\omega) = \omega^2 B_y^2 S_f(0, \omega) \left[\frac{\int [u'(z)]^2 dz}{\omega^4 |m_t|^2} + k_t^2 \mathrm{Av}\{|U(k_t)|^2\} \frac{S_y(\omega)}{S_f(0, \omega)} \right]$$

(26)

The magnitude of $\mathrm{Av}\{|U(k_t)|^2\}$ depends upon two things. On the one hand, if the profile is very smooth, then U(k) is given asymptotically for large k by (Lighthill, [5])

$$U(k) \sim - \frac{1}{k^2} \sum_n \Delta u'(z_n) e^{-ikz_n} ,$$

(27)

where $\Delta u'(z_n)$ is the jump in $u'(z_n)$ at the point of discontinuity z_n and the summation includes all points of discontinuity. Thus $\mathrm{Av}\{|U(k)|^2\}$ is

approximately

$$Av\{|\tilde{U}(k)|^2\} \sim \frac{1}{k^4} \sum_n |\Delta u'(z_n)|^2 .$$ (28)

On the other hand, if the profile is "rough" due, for example, to variations in the turns density or in the core permeability, then $|U(k)|$, for k not close to zero, can be much bigger than (27) predicts. For, expressing the actual rough profile $u_r(z)$ as

$$u_r(z) = u(z)[1 + \epsilon(z)] ,$$ (29)

where $\epsilon(z)$ is the "fractional perturbation" of the nominally smooth profile $u(z)$, then one can show that the expected value of $|U(k)|^2$ is augmented by the term $S_\epsilon(k)\int u^2(z)dz$. Here $S_\epsilon(k)$ is the spectral density of $\epsilon(z)$ and is defined as the Fourier transform of the correlation function of $\epsilon(z)$, which in turn is the expected value of $\epsilon(z)\epsilon(z+\zeta)$. It is assumed that $\epsilon(z)$ has zero mean and is statistically uniform and stationary in z.

The final general expression, therefore, for the motion-induced ENF of an antenna for which $u(z)$ is continuous but $u'(z)$ has discontinuities at z_n $(n=1, 2, \ldots)$ is $S_v(\omega)/\ell_e^2$ or

$$S_e(\omega) = \frac{\omega^2 \delta^2 B_y^2 S_f(0,\omega)}{2\int[u(z)\,dz]^2} \left[\frac{\int[u'(z)]^2 dz}{\omega^4 |m_t|^2} + \frac{\sum_n |\Delta u'(z_n)|^2}{k_t^2} \frac{S_v(\omega)}{S_f(0,\omega)} \right.$$

$$\left. + k_t^2 S_\epsilon(k_t) \int u^2(z)\,dz \frac{S_v(0,\omega)}{S_f(0,\omega)} \right] .$$ (30)

If the profile is nominally the ideal one defined by (22), then $\int u(z)dz$ is $4\ell u_o(0)/3$, $\int[u'(z)]^2 dz$ is $8u_o^2(0)/(3\ell)$, $\sum_n |\Delta u'(z_n)|^2$ is

$8\, u_o^2(0)/\ell^2$ and $\int u^2(z)\,dz$ is $16\,u_o^2(0)\ell/15$, so that (30) becomes

$$S_e(\omega) = \frac{3}{4\ell^3}\left(\frac{\delta B_y}{\omega|m_t|}\right)^2 S_f(0,\omega)\left[1 + \left\{\frac{3}{k_t^2\ell} + \frac{2}{5}k_t^2\ell^2 S_e(k_t)\right\}\frac{\omega^4 m^2 S_y(\omega)}{S_f(0,\omega)}\right].$$

(31)

By comparing this with the simple "long, smooth profile" formula given by (23), one sees that as the antenna becomes shorter, a correction term proportional to ℓ^{-4} will eventually be significant, and that the effect of profile roughness is to add a correction term proportional to the spectral density of the relative roughness and to ℓ^{-1}. Since the long, smooth profile term is $O\{\ell^{-3}\}$, and the "shortness" correction is $O\{\ell^{-4}\}$, this third roughness term will eventually dominate when the antenna is made arbitrarily long.

A further significant difference between the correction terms for shortness and for roughness on the one hand, and the long, smooth profile term on the other, is that the former are sensitive to the stiffness and absorption properties of the cable. To take simple account of this fact, it is convenient to define a mechanical Q-factor for transverse cable vibration as follows

$$Q_t = \frac{1}{2k_t}\int\left|\frac{H_t(k,\omega)}{H_t(0,\omega)}\right|^2 dk.$$

(32)

On the assumption that $S_f(k,\omega)$ is essentially constant over the range of k for which $H_t(k,\omega)$ has significant magnitude, Q_t is equal to $(\pi/k_t)\omega^4|m_t|^2 S_y(\omega)/S_f(0,\omega)$, so that (31) can be rewritten

$$S_e(\omega) = \frac{3}{4\ell^3}\left(\frac{\delta B_y}{\omega|m_t|}\right)^2 S_f(0,\omega)\left\{1 + \frac{3Q_t}{\pi k_t\ell} + \frac{2k_t^3\ell^2 Q_t}{5\pi}S_e(k_t)\right\},$$

(33)

and this formula applies to the nominally parabolic profile. The Q_t is a function of frequency and tension. A graph of Q_t, calculated for a specimen of the standard 0.65" D foamed-polyethylene buoyant antenna cable, is given in Appendix I, together with a similar graph of k_t.

Equation (33) shows that if $S_f(0, \omega)$ is known, then by calculating k_t and Q_t from measured mechanical properties of the cable, one can calculate the motion-induced ENF of an H-field antenna of given length and profile roughness. $S_f(0, \omega)$ can be estimated from boundary layer data (see Appendix D) or calculated once and for all from measurements of the vibration of a towed cable in a towing tank. Thus (33) frees one from the necessity of carrying out an expensive and time-consuming submarine test for each modification of the antenna design.

For the envisioned operational antenna length, $k_t \ell$ is very much larger than Q_t (see Appendix I), and so the "profile-shortness" correction term in (33) is small compared with unity. The "profile-roughness" correction term can be very much greater than unity, however. Since both this ENF and the motion-induced ENF of the E-field antenna are proportional to ℓ^{-1} (see Appendix G), a criterion for the profile smoothness for the H-field antenna can be obtained which is independent of ℓ. Thus, if the "profile-roughness" part of the motion-induced ENF of the H-field antenna is to be no greater than the motion-induced ENF of the E-field antenna, then

$$k_t S_\varepsilon(k_t) \leq \frac{5\pi}{36^2 k_t^2 Q_t} \qquad (34)$$

This criterion may be difficult to satisfy in practice, since both $k_t\delta$ and Q_t are numerically large.

Since the bending stiffness and mass distribution of an actual cable are not absolutely constant but vary slightly from point-to-point along the cable, and since the "profile roughness" is a serious noise source, the question arises of whether there should be a "cable-properties-variation" term in addition to the two other correcting terms in (33). It is easy to see, however, that such a term is negligible compared with the "profile roughness" term. For if the profile is perfectly smooth, then the variation of the cable properties has no effect, because the cancellation effect is a purely geometrical one depending only on the assumption that the disturbance attenuates as it propagates away from the disturbing force. Thus the "cable-properties-variation" term arises only if the profile is rough and so represents a perturbation of a correction. It is, therefore, negligible.

If the long, smooth profile condition can be achieved, then the advantage of using a parabolic rather than a uniform profile can be very great. For, from (12) and the definitions of ℓ_e and Q_t (Eqs. (2) and (32)), one deduces that the motion-induced ENF of an H-field antenna with a uniform profile is

$$S_e(\omega) = \frac{k_t Q_t}{4\pi \ell^2} \left(\frac{\delta B_y}{\omega |m_t|} \right)^2 S_f(0,\omega) . \qquad (35)$$

34

Thus, from (35) and (23), one sees that the uniform profile generates more noise by the factor $Q_t k_t \ell/(3\pi)$ than the purely parabolic profile. For envisioned operational antenna lengths incorporated in the current design of antenna cable, this factor can be of the order of 10^4 or 40 dB, as reference to Appendix I will verify.

As for the effect of cable diameter on motion-induced ENF, equation (33), together with the expression for $S_f(0,\omega)$ given in Appendix D, shows that the long-smooth-profile approximation is proportional to the inverse square power of the cable radius (assuming the cable density does not vary). On the other hand, the profile-roughness contribution is proportional to the inverse seven-halves power of the cable radius, if the bending stiffness is the dominant restoring force. For low frequencies and large tensions, however, when the cable tension provides a considerable part of the restoring force, the precise law is difficult to state simply. This is because an increase in radius increases the bending stiffness and therefore also increases the mechanical damping. Thus the Q is a complicated function of diameter. In the extreme case of very high tension, since the tension itself is proportional to cable radius, the profile-roughness contribution to the motion-induced ENF is proportional to the inverse half-power of the cable radius. But, in practice, the tension would be too small, and the frequency and diameter too large, for this behavior to be observed.

V. Magnetostrictive Noise

In Section I the manner in which magnetostrictive noise is generated was described. The various techniques for reducing it (selection of core material, using a degaussing current, stress-relieving mechanical construction and profile shaping) were also briefly mentioned. In this Section the two latter techniques are examined in greater detail.

When the antenna core is axially strained, there is a concomitant "magnetic strain" in the axial geomagnetically-induced bias flux density B_o:

$$\frac{\Delta B}{B_o} = \epsilon \frac{\Delta \ell}{\ell} . \tag{36}$$

Particular ferromagnetic alloys exist for which the "strain-ratio" ϵ is minimized, but in general it is a large number -- about 10^4, for example, for 45 Permalloy [1, p. 618].

If the axial displacement of a point on the cable from its rest position be denoted by $x(z,t)$, then the axial strain is $\partial x(z,t)/\partial z$ and so the change of flux linkage is given, from (36), by

$$d\Phi = B_o \epsilon N A \, \partial x(z,t)/\partial z ,$$

where N is the turns density of the antenna winding and A is the area of the ferromagnetic core. Thus the total magnetostrictive noise voltage is given by

$$v(t) = \int \epsilon B_o N A \frac{\partial^2 x(z,t)}{\partial z \partial t} \, dz . \tag{37}$$

In the frequency domain, this is

$$V(\omega) = -i\omega \int \epsilon B_o N A \frac{\partial X(z,\omega)}{\partial z} \, dz . \tag{38}$$

Now the axial strain is present in the form of longitudinal mechanical waves travelling along the cable. The attenuation of these waves is relatively small (see Appendix I) and so disturbances generated outside the antenna region travel into and through it. Thus $X(z,\omega)$ has' the form $X(0,\omega) \exp(i k_o z)$ where k_o is the (complex) wave number for longitudinal

36

mechanical waves. Thus (38) can be written

$$V(\omega) = \omega k_o X(0, \omega) \int \varepsilon B_o N A e^{ik_o z} dz . \tag{39}$$

In practice, the quantities ε, B_o and μ_a are likely to be constant along the antenna. Then, since $u(z)$ has been defined in Section IV to be the product $\mu_a N A$, (39) can be written as

$$V(\omega) = \omega k_o X(0, \omega) \frac{\varepsilon B_o}{\mu_a} U(-k_o) , \tag{40}$$

where $U(k)$ is the Fourier transform of $u(z)$. The magnetostrictive ENF spectral density is therefore given by dividing $V(\omega)$ by ℓ_e from (2) and squaring. That is

$$S_e(\omega) = \frac{1}{2} \left(\frac{\omega B_o \delta \varepsilon}{\mu_a} \right)^2 S_x(\omega) \left| \frac{k_o U(-k_o)}{U(0)} \right|^2 , \tag{41}$$

where $S_x(\omega)$ is the power spectral density of $x(0, t)$.

Equation (41) shows that the antenna sensitivity profile $u(z)$ should be shaped to minimize the ratio $|U(-k_o)/U(0)|$. Since the antenna is likely to be long compared with the wavelength of the longitudinal waves (i.e., $|k_o \ell| \gg 1$), the value of $U(-k_o)$ is largely determined by the magnitude of the lowest-order discontinuity of the function $u(z)$, while $U(0)$ is the area under the curve. Much the same considerations apply here, therefore, as did to the reduction of motion-induced noise. The profile should be as long and as smooth as possible. Here, however, the reduction in noise obtained by going from a uniform to a tapered profile is not as dramatic, because the wavelength of the longitudinal waves is longer than that of the

37

transverse, but further improvement is possible by removing the discontinuity in the slope of u(z) at $\pm\ell$.

To be specific, Table II shows the formulas for $U(k)/U(0)$ when the lowest-order discontinuity in u(z) occurs in its zeroth, first and second derivative, and also their asymptotic form.

Table II

Three Fourier Transform Pairs

u(z)		U(k) / U(0)
$|z| > \ell$	$|z| \leq \ell$	
0	1	$\dfrac{\sin k\ell}{k\ell} \sim \dfrac{\sin k\ell}{k\ell}$
0	$1 - z^2/\ell^2$	$- \dfrac{3}{(k\ell)^2} \left\{ \cos k\ell - \dfrac{\sin k\ell}{k\ell} \right\} \sim - \dfrac{3 \cos k\ell}{(k\ell)^2}$
0	$(1 - z^2/\ell^2)^2$	$- \dfrac{15}{(k\ell)^3} \left\{ \sin k\ell + 3 \dfrac{\cos k\ell}{k\ell} - 3 \dfrac{\sin k\ell}{(k\ell)^2} \right\} \sim - \dfrac{15 \sin k\ell}{(k\ell)^3}$

Since $|k_o|$ is of the order of 0.15 (see Appendix I) and 2ℓ might be as much as 300 m, $|k_o\ell|$ is of the order of 10 or 20. Thus equation (41), together with the asymptotic form given for $U(k)/U(0)$ in Table II, shows that reductions of the magnetostrictive ENF of tens of decibels are possible by smoothing the sensitivity profile.

The noise can also be reduced by reducing the cable vibration level $S_x(\omega)$. Using a mechanically more absorptive cable or using vibration isolators in the cable between the antenna and the source of the vibration are

38

ways of achieving this. If this procedure is pursued far enough, the longitudinal waves in the antenna region will then be generated locally by the force fluctuations in the turbulent boundary layer, as is already the case for transverse waves. Using the method of the previous Section, one can show that the magnetostrictive ENF is then given by

$$S_e(\omega) \approx \frac{1}{2} \left(\frac{\omega B_o \delta \gamma}{\mu_a} \right)^2 S_s(0,\omega) \ \frac{1}{2\pi} \int \left| \frac{k\, U(k)}{U(0)} \right|^2 \left| H_\ell(k,\omega) \right|^2 dk$$

(42)

where $S_s(k,\omega)$ is the double-spectral density of the longitudinal shear forces on the cable and $H_\ell(k,\omega)$ is the spectral transfer function relating axial motion to shear force (see Appendices D and E).

The factors in the integrand here have the same general features as the corresponding ones do in the case of transverse waves (see Fig. 7). However, the wavelength of the longitudinal waves is so much longer than that of the transverse waves that the peak in the $\left| H_\ell(k,\omega) \right|^2$ function occurs at a much smaller value of k. The magnitude of $\left| U(k) \right|^2$ is therefore in general bigger there. Thus the contribution to the integral from the peak in $\left| H_\ell(k,\omega) \right|^2$ is much greater than that from the peak in $\left| U(k) \right|^2$. The equation can therefore be approximated as

$$S_e(\omega) \approx \frac{1}{2} \left(\frac{\omega B_o \delta \epsilon}{\mu_a} \right)^2 S_s(0,\omega) \left| \frac{k_\ell U(k_\ell)}{U(0)} \right|^2 \frac{1}{2\pi} \int \left| H_\ell(k,\omega) \right|^2 dk$$

(43)

where $\pm k_\ell$ are the values of k at which the peaks of $\left| H_\ell(k,\omega) \right|^2$ occur. This is more conveniently expressed in terms of the mechanical Q-factor for longitudinal cable vibration, defined as

39

$$Q_\ell = \frac{1}{2k_\ell} \int \left| \frac{H_\ell(k,\omega)}{H_\ell(0,\omega)} \right|^2 dk. \tag{44}$$

Then, since $H_\ell(0,\omega) = 1/(\omega^2 m_\ell)$, where m_ℓ is the effective longitudinal vibrating mass per unit length of cable, (43) can be rewritten as

$$S_e(\omega) \approx \frac{1}{2\pi} \left(\frac{B_o \delta \epsilon}{\mu_a \omega |m_\ell|} \right)^2 \left| \frac{k_\ell U(k_\ell)}{U(0)} \right|^2 k_\ell Q_\ell S_s(0,\omega) . \tag{45}$$

This formula is very similar to (41), but now the driving forces and cable properties appear explicitly. A general expression for Q_ℓ in closed form is given in Appendix E and a graph of Q_ℓ, for a specimen of the standard 0.65"D foamed-polyethylene buoyant antenna cable, is presented in Appendix I, together with a similar graph of k_ℓ.

Equation (45) shows that if $S_s(0,\omega)$ is known, then the magnetostrictive ENF of an H-field antenna can be estimated from mechanical and electrical laboratory experiments performed on the antenna [10]. Since the shear forces on the cable depend only on its diameter (assuming it has a smooth enough surface), then the ENF estimate obtained in this way would be a lower bound. Disturbances propagating into the antenna region (from sources of vibration associated with the towing vessel) would generate additional ENF, but could in principle be made negligible by using a long enough cable, using a mechanically more lossy cable or by installing a mechanical isolator forward of the antenna region.

Equations (41) and (45) suggest other means of reducing the magnetostrictive ENF. The bias flux density B_o can be minimized by

driving a degaussing current through the antenna winding [4] and ϵ can be reduced both by careful selection of the core material and by constructing the core in such a manner that the core strain is much less than the cable strain. Increasing the diameter is also a possibility. Assuming that $S_s(0,\omega)$ has the same behavior with radius as does $S_f(0,\omega)$ (see Appendix D), one can deduce from (45) that the magnetostrictive ENF power is inversely proportional to radius squared, other things remaining constant. A somewhat more rapid reduction with radius than this would be expected, however, because the strength in tension of the cable should be proportional to the radius of the cable. Thus the restoring force for mechanical vibration is proportional to a , but the mass to be restored, per unit length, is proportional to a^2. Thus k_ℓ is proportional to $(a^2/a)^{\frac{1}{2}}$ or $a^{\frac{1}{2}}$, and since for a parabolic sensitivity distribution, $k\,U(k)/U(0)$ is asymptotically proportional to k^{-1}, then an additional factor of $a^{-\frac{1}{2}}$ appears in the behavior with radius of the magnetostrictive ENF. A stiffer, more lossy cable would also result in a lower magnetostrictive ENF.

The possibility of using a strain relief core construction deserves a little further attention in the case in which the core is a helical wrap of ferromagnetic tape By considering the deformation of a helical line in a homogeneous circular cylinder as the cylinder stretches, one finds that the strain $\delta\ell/\ell$ of the helical line (i.e., increase in length per unit length measured along the helix) is given by

$$\frac{\delta\ell}{\ell} = [\, 1 - (1+\upsilon)\sin^2\theta\,]\,\frac{\delta z}{z} \qquad (46)$$

41

where υ is Poisson's ratio for the material of the cylinder, θ is the helix angle and $\delta z/z$ is the axial strain of the cylinder. Thus when the helix angle is zero (which means the helical line degenerates into a straight line parallel to the axis), the line and cylinder strain by the same amount. If, on the other hand, the helix angle is $\arcsin (1+\upsilon)^{-\frac{1}{2}}$, then the helical line maintains a constant length as the cylinder strains. For incompressible materials, $\upsilon = 1/2$, and the corresponding "zero-strain" helix angle is $\arcsin \sqrt{2/3}$ or about $55°$.

Whether it is desirable to make use of this "zero-strain" helix condition depends upon the relative levels of the magnetostrictive and thermal ENF's. The thermal ENF power is proportional to $(\cos \theta)^{-4}$, for a given core weight per unit length. This means that taking θ equal to $55°$ rather than $0°$ increases the thermal ENF by nearly 10 dB.

In practice, the core-tape is not an infinitesimally thin line but has a finite cross-sectional area. This means that the helix angle varies across the radial thickness of the core-tape (since $\tan \theta = 2\pi r/p$, where r is the radius and p the pitch) so that there will be a varying linear strain across the radial thickness. Presumably, by arranging for θ to assume its "zero-strain" value at the radius of the midpoint of the tape thickness, the net strain can be minimized. Other effects, such as shear strain across the width of the core-tape and helix distortion due to the difference in mechanical stiffness between the core material and its surroundings, may also need to be taken into account.

The possibility of magnetostrictive noise being generated by transverse mechanical waves should not go without mention. However, if the geomagnetic field is wholly axial, the geometry has rotational symmetry. Then, the noise voltage generated by bending the antenna would be independent of the azimuthal direction in which the bend occurred. The voltage cannot therefore be linearly related to the transverse displacement, but must depend on its square or some higher even power. It is therefore of at least second order, and since the transverse displacement is very small to begin with, it should be negligible compared with the longitudinally generated magnetostrictive noise. The geometry is no longer rotationally symmetric if a transverse component of the geomagnetic field exists. In that case, however, the core geometry is unfavorable for the induction of any substantial bias flux density into the core, and what does exist is on balance, purely transverse (the axial components of the induced flux density are in opposite directions on opposite sides of the core, if the core is helically wrapped). Thus the only magnetostrictive effect of bending is a change in the transverse flux density, which does not couple with the winding. Another rotationally antisymmetric geometry is one in which the geomagnetic field is wholly axial but the antenna axis does not coincide with the neutral axis of the whole cable. Then, being offset from the no-strain axis, the core is subject to axial strain as a result of pure bending. It is probably important, therefore, to keep the axes of the antenna and of the whole cable coincident.

VI.   Barkhausen Noise

As the towing vessel changes its heading, the smoothly changing axial component of the geomagnetic field is not accompanied by an equally smooth variation in the resulting flux density it induces in the antenna core. The flux density changes in a sequence of abrupt jumps known as Barkhausen discontinuities [1, p. 524], which, in turn, induce a wide-spectrum noise voltage in the antenna winding.

This noise is the most difficult of the known noise sources to handle quantitatively. This is because the Barkhausen noise generated by different ferromagnetic materials bears no obvious relation to one permeability, and while Mumetal, for example [8, ?], has been measured to have very low Barkhausen noise when soft, the noise rises substantially when the material has undergone some work hardening. This work hardening would occur, in particular, in the fabrication of a helical tape core.

The effect of core area on Barkhausen ENF is probably small, although it has not been investigated directly. This is because the Barkhausen jumps tend to occur in clusters as a macroscale effect [8], so that the bigger the core cross-section, the bigger the cluster involved. Thus, the noise increases, but the signal sensitivity does also. The clustering effect would not, however, extend far along the length of the core and so one would expect the flux density variation to be statistically independent at widely separated points along the antenna. Thus Barkhausen ENF power is expected to be proportional to the inverse first power of antenna length.

44

A direct method of preventing Barkhausen noise is to maintain the induced flux density in the antenna core as constant as possible. Thus an automatically controlled degaussing current, which maintains antenna sensitivity and reduces magnetostrictive noise can also reduce the Barkhausen noise. Measurements of the Barkhausen noise caused by applied field changes of different rates enable one to specify the performance required from the control loop [4]. For noisy materials, the open loop gain of the control loop may turn out to be unrealistically large.

VII. Some Experimental Results

In Appendix D, a comparison is made between the measured noise of a long E-field antenna and the motion-induced noise one would expect to measure if the antenna motion were due to the pressure fluctuations of the turbulent boundary layer. It was found that the predicted and measured noises follow the same law with both frequency and speed (namely, the noise power spectral density is proportional to the fifth power of towing speed and inverse fourth power of frequency). On the other hand, there is a constant difference between the predicted and measured level of some 16 dB. This may be due to the fact that the pressure fluctuation data used in the estimate came from the literature in which only flat or near-flat surfaces have been dealt with.

Further evidence that the transverse mechanical waves on the cable arise from the turbulence in the boundary layer comes from measurements made with towed cables equipped with strain gages and accelerometers. It was found that the cable curvature (measured with diametrically opposed

-45

strain gages) and acceleration at different points along the cable were consistent with the hypothesis that a statistically uniform driving mechanism existed over the whole cable length. The only other possibility, that the cable motion is excited near the tow-point or near the free-end and then propagates as transverse waves to the rest of the cable, cannot be reconciled with the measurements. This is because the attenuation of transverse waves is so great (see Appendix I) that substantially different vibration levels would be observed by two sensors spaced, say, a couple of hundred feet apart. No such differences were observed.

For longitudinal waves, the situation is less clear. Shear-stress fluctuations in turbulent boundary layers have not apparently been treated in the open literature, so that no predictions can be made of the role they play. In addition, the attenuation of longitudinal waves is small enough (see Appendix I) that the effect of tow-point disturbances may well be observable along the whole cable length.

However, data obtained with strain gages show two separate phenomena which suggest that local (i.e., boundary-layer) excitation is, in fact, what predominates. The first phenomenon is the observation of a marked standing-wave pattern near the tow point. This means that the energy is not entering the cable at the tow point, for if this were the case, the energy would be flowing unidirectionally away from the tow point and no standing waves would be observed. Thus the energy is generated on the cable somewhere else and then propagates along to the tow point where it is reflected back again to interfere with the incident energy and form

46

standing waves. The second phenomenon is that the strain amplitude in the cable is essentially uniform over its whole length. Thus the exciting source must be well distributed and statistically uniform. (It is true that the attenuation per meter of longitudinal waves is small, but the cable is so long that an easily measurable difference in level would be present if the energy were generated at one location.)

The strain-gage data, together with the theory developed in the previous sections, allow one to predict the noise voltages generated by the different antennas tested experimentally. Considering first motion-induced noise, since cable curvature is the second derivative with respect to distance of cable displacement, then the curvature spectral density $S_c(\omega)$ is given closely by $S_y(\omega)/k_t^4$, where $S_y(\omega)$ is the displacement spectral density. Therefore, combining (G6) with (E12) one finds for the motion-induced voltage spectrum $S_v(\omega)$ of a long E-field antenna

$$S_v(\omega) = \ell_e^2 S_e(\omega) = \frac{2\ell \pi B_y^2 \omega^2}{k_t^5 Q_t} S_c(\omega) \tag{47}$$

where k_t and Q_t are to be evaluated using the cable tension appropriate for the position along the cable at which the curvature is measured.

Similarly, by combining (35) with (E12), and using the results of Appendix H, one finds for the motion-induced voltage spectrum of a long H-field antenna with a uniform profile

$$S_v(\omega) = \ell_e^2 S_e(\omega) = \frac{1}{8} \left(\frac{\delta \ell_e B_y \omega}{\ell} \right)^2 \frac{[k_t Q_t]_\ell + [k_t Q_t]_{-\ell}}{[k_t^5 Q_t]_g} S_c(\omega) \tag{48}$$

47

where the suffix ℓ, $-\ell$ or g means that the enclosed quantity is to be evaluated using the tension appropriate for the position along the cable of the two ends of the antenna (ℓ & $-\ell$) or of the strain gages measuring the curvature (g).

In Fig. 13, graph a) shows the curvature spectrum measured with a strain-gage pair placed 400 feet from the free end of a cable being towed at 12 knots. In graph b), the result of applying (47) to this curvature spectrum to derive the motion-induced noise voltage of a 300-meter long E-field antenna towed at 12 knots is compared with the "measured" E-field antenna noise voltage. The "measured" 12 knot curve was actually obtained by lowering the 14 knot data of Fig. 3 by 3.35 dB, since the noise voltage follows a speed-to-the-fifth-power law. Graph c) shows the result of applying (48) to the curvature spectrum of graph a) to derive the motion-induced noise voltage of an 800-foot long H-field antenna having a uniform sensitivity profile and an effective length of 5.3 meters at 45 Hz. The measured curve was obtained with the RCA Helix III antenna. For both derivations, the values of k_{ι} and Q_{ι} were obtained from Figs. 8, 9 and 12, B_y was assumed to be 0.5×10^{-4} weber m^{-2} (0.5 gauss) and the skin-depth was calculated using an ocean conductivity of 4 mho/m.

It should be noted first that the calibration of the strain gages was calculated solely from their nominal off-set from the cable axis. In fact, they are somewhat less sensitive than such a procedure would indicate because the physical modification necessary for installation stiffens the cable locally. Also, the RCA antenna cable was structurally different from the cable having the measured properties summarized in Appendix I.
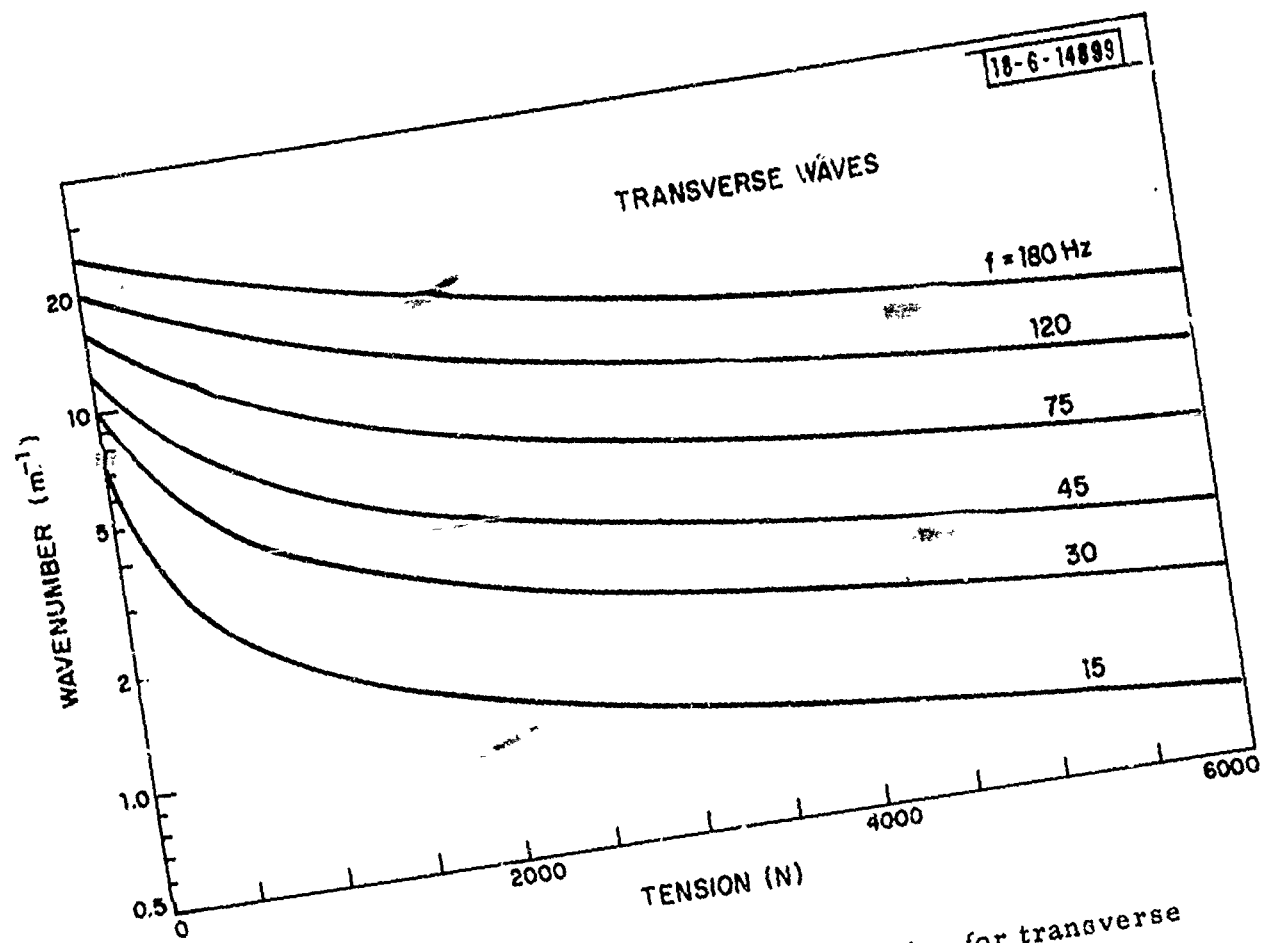
Fig. 8. Wavenumber k_t vs frequency and tension for transverse mechanical waves on the 0.65 inch O.D. buoyant cable.
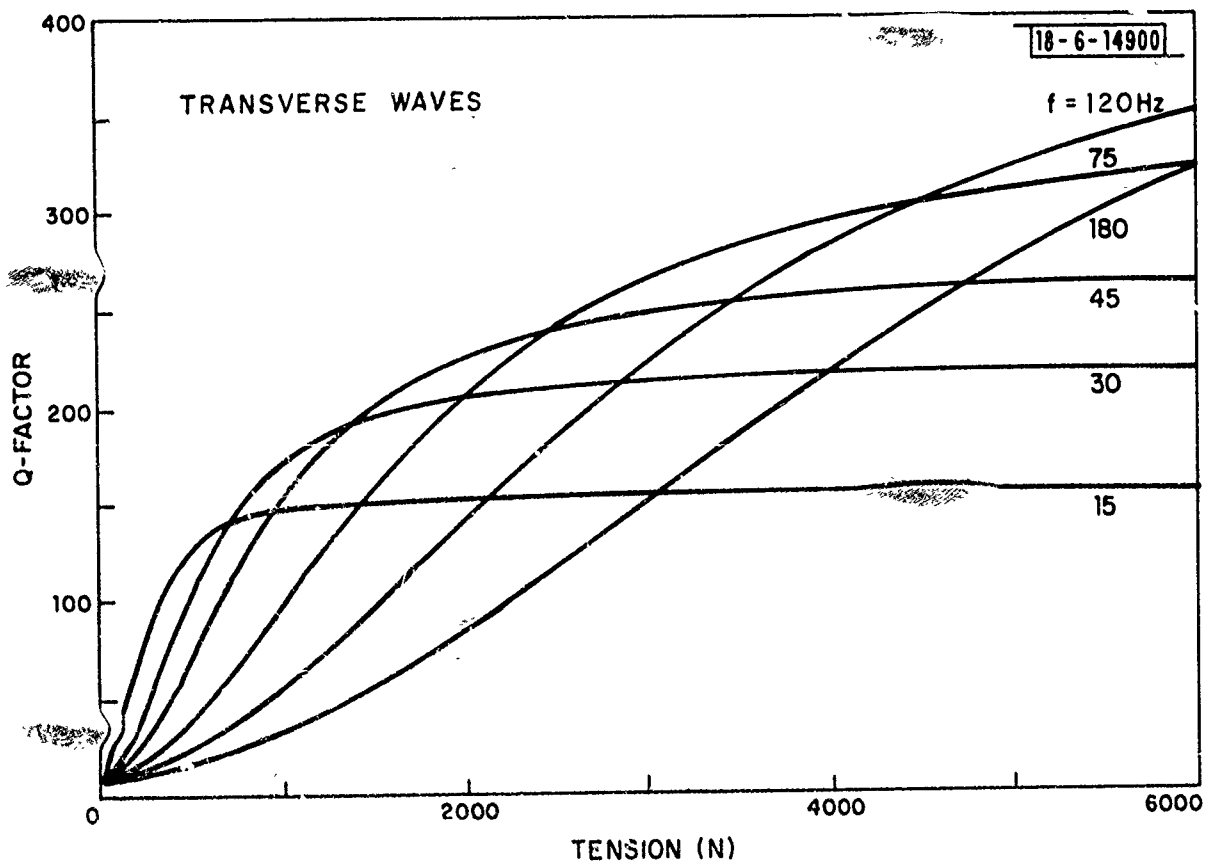
Fig. 9. Mechanical Q-factor Q_t vs frequency and tension for transverse waves of the 0.65 inch O. D. buoyant cable.

18-6-14901

TRANSVERSE WAVES

f = 180 Hz

120

75

45

30

15
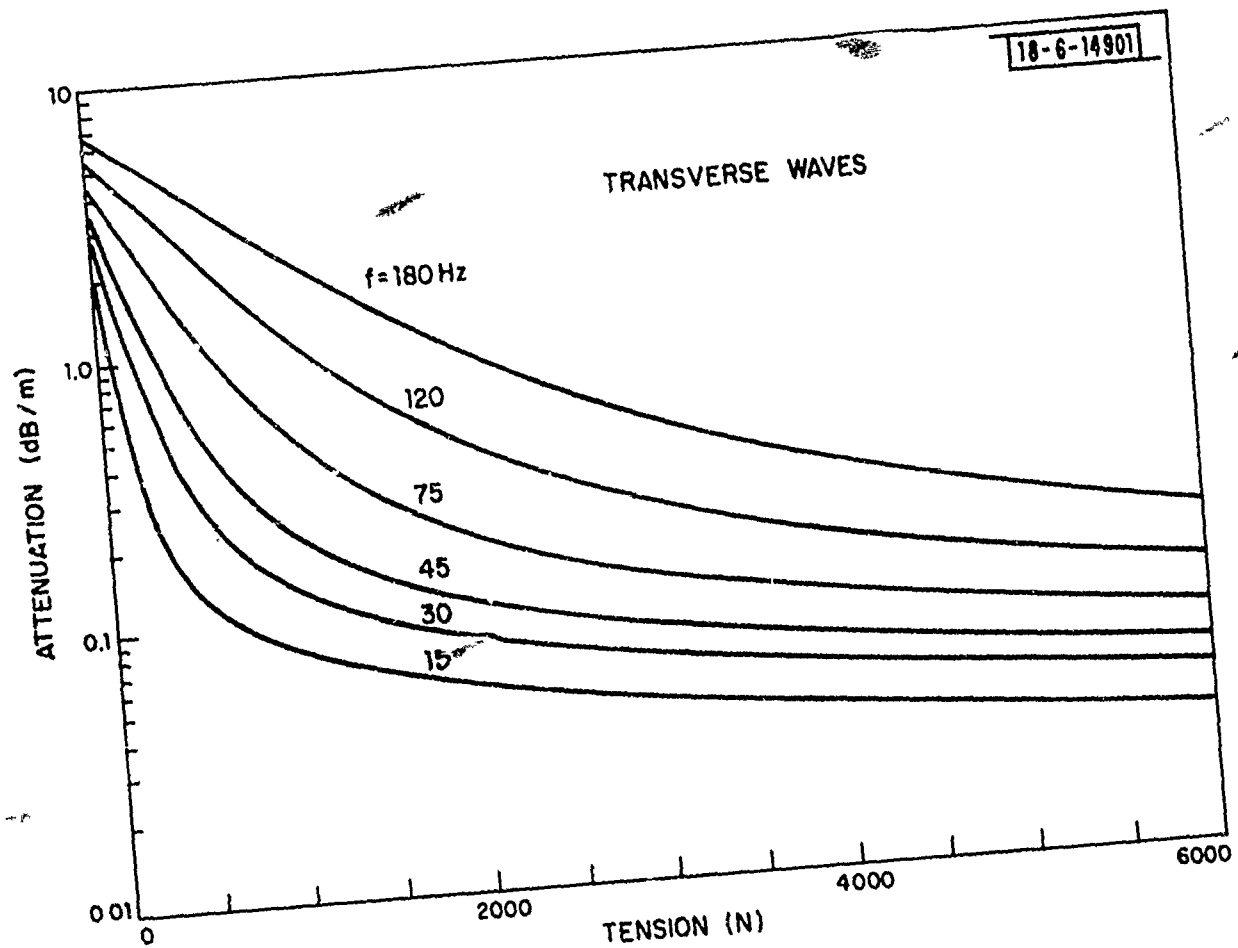
Fig. 10. Attenuation α_t vs frequency and tension for transverse
mechanical waves on the 0.65 inch O. D. buoyant cable.

51

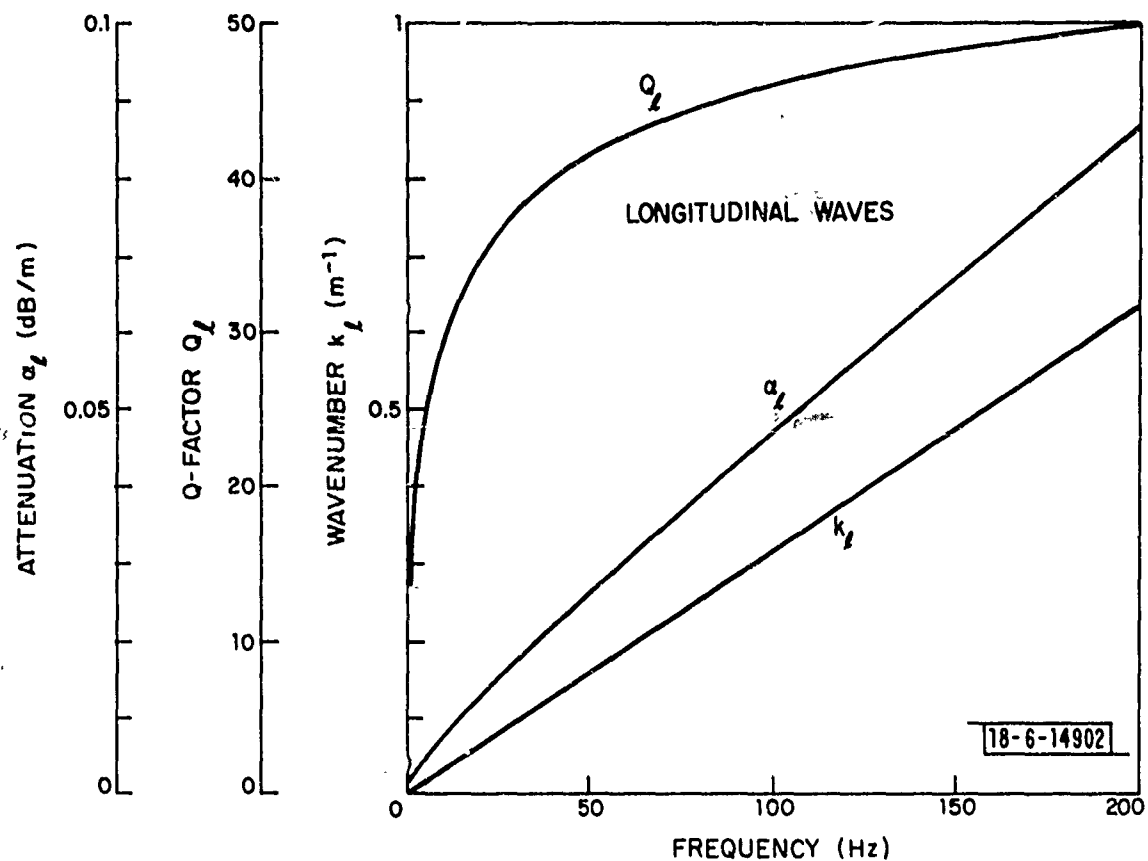Fig. 11. Wavenumber k_ℓ, Q-factor Q_ℓ and attenuation α_ℓ vs frequency for longitudinal mechanical waves on the 0.65 inch O. D. buoyant cable.
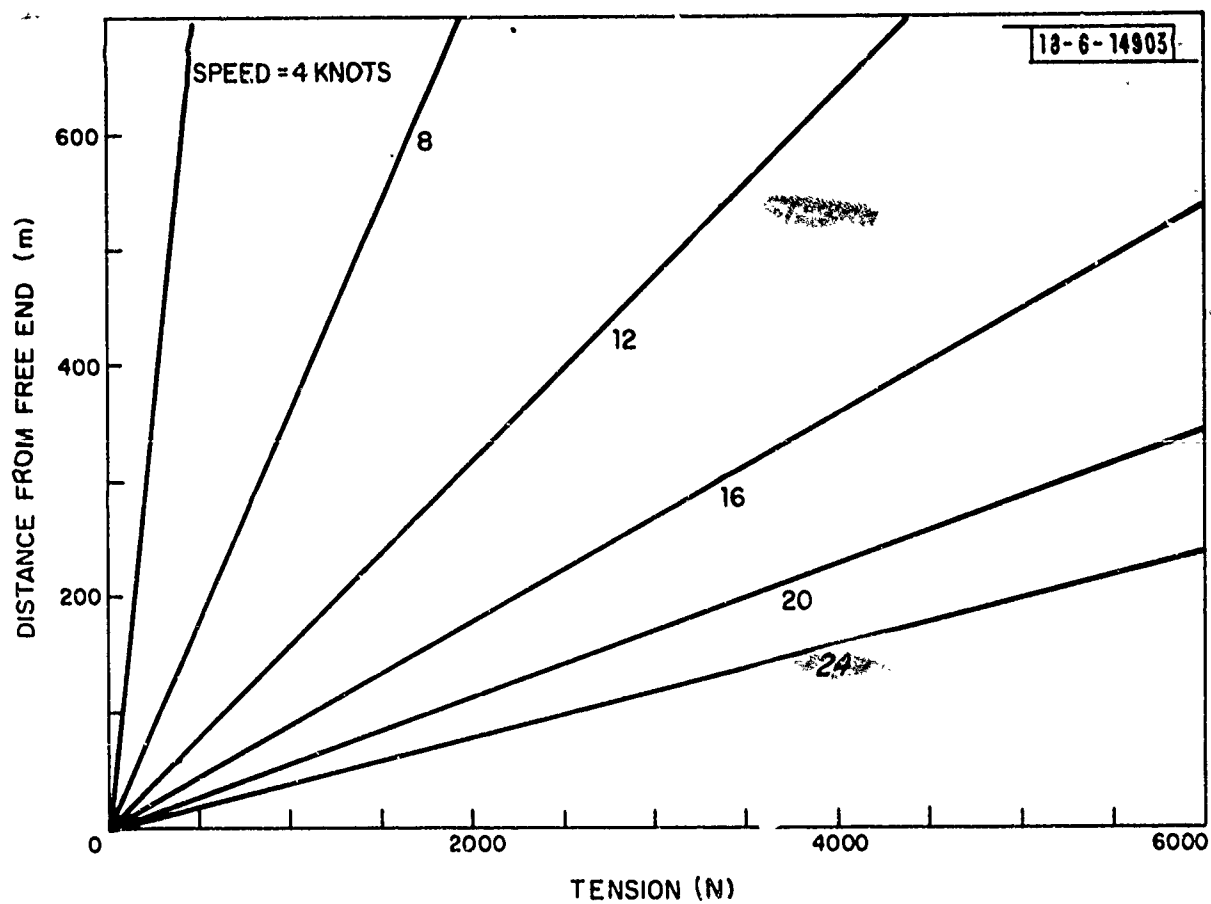
52

Fig. 12. Cable tension as a function of distance from free end and speed for 0.65 inch O. D. buoyant cable.
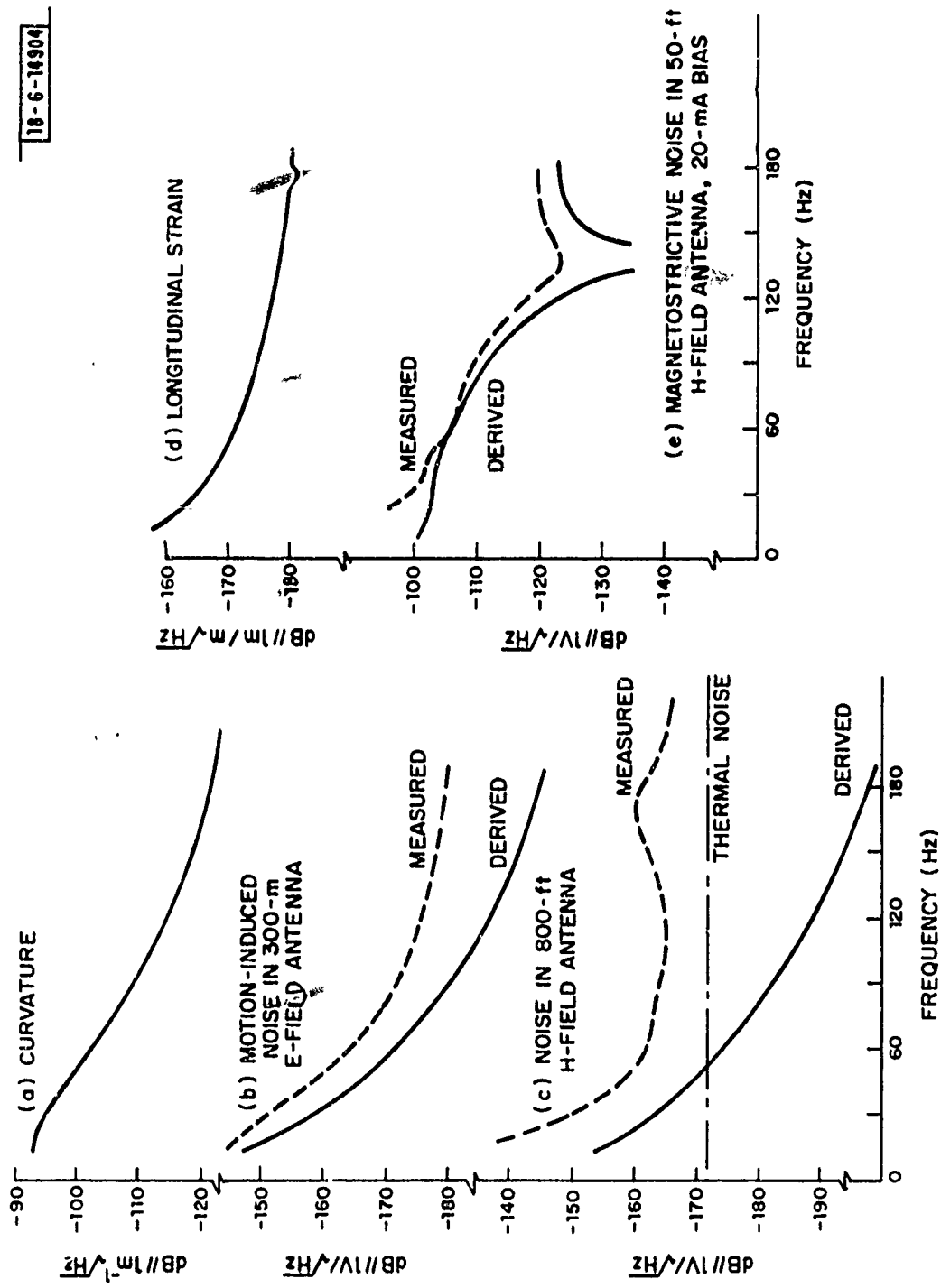
Fig. 13. Directly-measured noise voltages compared with those derived from strain-gage data, all at 12 knots.

54

In view of these differences, therefore, the agreement between derived and measured noises in graphs b) and c) is not bad. Until thermal noise takes over at higher frequencies, the E-field antenna noise level is consistent with the hypothesis that it is motion-induced, and the same applies to the H-field antenna, except that it appears to be the profile roughness contribution which takes over from the long-profile term at higher frequencies. No sensitivity-profile data is available for the RCA antenna and so no estimate can be made of the profile roughness contribution.

The remaining two graphs in Fig. 13 concern longitudinal waves and their generation of magnetostrictive noise. Graph d) is the longitudinal strain spectrum measured with the same two gages used to obtain graph a), and graph e) is the corresponding prediction of the magnetostrictive noise voltage spectrum together with the actual measured spectrum for the Lincoln Laboratory 50-foot long H-field antenna.

The prediction was made in the following way. The magnetostrictive noise voltage spectrum $S_v(\omega)$ is given, from (41) as

$$S_v(\omega) = \ell_e^2 S_e(\omega) = \frac{1}{2}\left(\frac{\omega B_o \delta \epsilon \ell_e}{\mu_a}\right)^2 S_x(\omega) \left|\frac{k_o U(-k_o)}{U(0)}\right|^2, \qquad (49)$$

in which, since the Lincoln Laboratory antennas have nominally parabolic profiles, $U(k)$ is given by the second line in Table II in Section V. But at the same strongly biased condition (20 mA) used for measuring the antenna noise, the strain sensitivity of a 2-foot long, single-core-bundle antenna element was found to be [10] 32 dB//1 V/unit strain at 45 Hz. Since the

effective length of the antenna element is $\ell_e/50$, then equation (49) can be written for the element as

$$32 = 10 \log_{10} \left\{ \frac{1}{2} \frac{90 \pi B_o \delta \varepsilon \ell_e}{50 \mu_a} \right\} , \qquad (50)$$

which establishes the value of the quotient $B_o \delta \varepsilon \ell_e/\mu_a$ in (49). (Strain is the length derivative of displacement, and $|k_o|$ is essentially equal to k_ℓ so that $|k_o|^2 S_x(\omega)$ can be replaced by the strain spectrum $S_\lambda(\omega)$, and for the element, for which $k_\ell \ell << 1$, $|U(-k_o)/U(0)|$ is essentially equal to unity.)

Using i) the value for $B_o \delta \varepsilon \ell_c/\mu_a$ established by (50), ii) the strain spectrum $|k_o|^2 S_x(\omega)$ from graph d) and iii) the formula for $U(k)$ given in the second line in Table II in Section V, one obtains from formula (49) the "derived" curve in graph e). To make the null in the "derived" curve coincide with the minimum of the measured curve, a value for the longitudinal wave speed was used which is 77% of that implied by the data given in Appendix I. This is not unreasonable, because at low tensions it was found that the cable is less stiff in stretching.

The remarkably close agreement between the "derived" and measured curves gives strong support to the theory of magnetostrictive noise generation.

No Barkhausen noise has apparently been observed under towing conditions, because other noises have always been dominant. Barkhausen noise data measured in the laboratory is available, however, in Ref. [4].

VIII. Conclusion

The previous sections have shown that an air-cored towed H-field antenna would be inconveniently large if its thermal ENF is to be low enough for it to approach the performance of the towed E-field antenna. In addition, an H-field antenna in the existing buoyant antenna cable would generate too much motion-induced ENF if it had a uniform sensitivity profile. Thus a ferromagnetic core and a shaped sensitivity profile appear to be necessary features. The introduction of the core, however, adds two more noise sources -- magnetostrictive and Barkhausen.

The theory developed to examine the various noise sources has been shown capable of predicting the noise voltages by combining cable vibration data with laboratory measurements on antenna samples. One particularly troublesome noise source has been revealed to be motion-induced noise contributed by "profile-roughness".

Since the available cable vibration data and theory indicate that all cable motion is excited by the stress fluctuations in the turbulent boundary layer, it would appear that using vibration isolators or towing further behind the boat would be ineffective in reducing cable vibration. Measures that would be effective include using a stiffer, more mechanically lossy cable and increasing its diameter. Reducing the sensitivity of the antenna to the vibration is accomplished by tapering its profile, making its profile as smooth as possible, using a degaussing current, using a stress-relieving core construction and choosing a core material low in magnetostriction and Barkhausen noise.

IX. Acknowledgements

APPENDIX A

IMMERSION EFFECT ON ANTENNA IMPEDANCE

An infinitely long solenoid carrying a current $I^{(e)}$ and immersed in a conducting medium induces in the medium a magnetic field given by

$$H = -\frac{i\sigma}{4} H_o^{(1)}(kr) I^{(m)} \tag{A-1}$$

at a distance r from the solenoid axis. Here, k is the wave number for propagation in the medium, defined as $\sqrt{i\omega\sigma\mu_o}$, and $I^{(m)}$ is the axial magnetic current equivalent to the energized solenoid, given by $I^{(m)} = -i\omega\mu_c A N I^{(e)}$, where μ_c and A are the permeability and cross-sectional area of the core. It is assumed that $I^{(m)}$ is uniform. (This formula is obtained by applying the principle of duality to the well-known [2] result $E = -\omega\mu_o H_o^{(1)}(kr) I^{(e)}/4$ for the electric field due to an axial electric current.)

At any radius r, this field is the field arising from all the cylindrical shells of current induced in the medium having radii larger than r. Thus the magnetic field within the solenoid arising from the external induced currents is uniform and given by setting r in (A.1) equal to r_m, the outside radius of whatever nonconducting jacket covers the solenoid.

Hence the voltage ΔV induced per unit length in the solenoid by the external currents is given by $-i\omega\mu_c A N H$, and the change in impedance per unit length by $\Delta V/I^{(e)}$. That is,

$$\Delta Z = \frac{i}{4}\omega^2\mu_c^2 A^2 N^2 \sigma H_o^{(1)}(kr_m)$$

The inductance per unit length L_0 is easily shown to be equal to $N^2 \mu_c A$, so that the impedance change, normalized with respect to the imaginary component of the self impedance, is

$$\frac{\Delta Z}{\omega L_0} = \frac{i}{4} \omega \sigma \mu_c A H_0^{(1)}(kr_m) .$$

Since the skin depth in the ocean at ELF is many meters whereas r_m is limited to one or two centimeters, the small-argument form of the Hankel function can be used to rewrite this as

$$\frac{\Delta Z}{\omega L_0} \sim \frac{\mu_c}{\mu_0} \frac{A}{\delta^2} \frac{1}{\pi} \left[\ln \frac{\delta}{\sqrt{2} r_m} - .577 + i \frac{\pi}{4} \right] . \quad (A-2)$$

At 45 Hz and for the typical value of σ of 4 mho/meter, the skin depth δ is 37.5 meters. Thus if A is one square centimeter or 10^{-4} meters, μ_c/μ_0 is 2×10^4 and r_m is 10^{-2} meters, then $\Delta Z/\omega L_0$ is about $(3.3 + i\, 0.36) \times 10^{-2}$. Hence the change in impedance is very small compared with the total impedance.

The thermal noise contribution of the water losses, expressed as an equivalent noise field (ENF) is given by $[4 k_b T_k \mathrm{Re}\{\Delta Z\}]^{\frac{1}{2}}$ divided by the effective length per unit length of the antenna, where k_b is Boltzmann's constant and T_k the temperature in degrees Kelvin. The effective length per unit length is, from (2), $\sqrt{2} \mu_c A N/(\delta \mu_0)$, so that

$$\mathrm{ENF} = \left\{ \frac{2}{\pi} k_b T_k \omega \mu_0 \left[\ln \left(\frac{\delta}{\sqrt{2} r_m} \right) - .577 \right] \right\}^{\frac{1}{2}} \quad (A-3)$$

is the ENF of a 1 meter length of the infinite solenoid and is proportional to $(\text{length})^{-\frac{1}{2}}$.

For the same assumptions as before, and for a temperature of 300° Kelvin, this works out to be -232 dBE (dBE denotes dB with respect to 1 volt per meter per $\sqrt{Hz}$). For a 300 meter length of the solenoid, therefore, the ENF contributed by the water losses is -257 dBE. This is lower than the total ENF of the trailed 300-meter E-field antenna (Fig. 3) by some 50 dB and so is not of concern.

This analysis of the effects of immersion has used as a model the infinitely long uniform solenoid. It is probably not accurate unless the antenna is many skin-depths long. However, since the effect has been shown to be very small and since the antenna length is likely to be a few skin depths long, one can safely assume that the effect on a real antenna is not accurately known but is still negligible.

APPENDIX B

OPTIMUM AIR-CORE ANTENNA

For an air-core antenna, the flux linking a turn of radius r is given by $\pi r^2 \mu_0 H_i$, so that the total flux linkage is the quantity $\pi r^2 \mu_0 H N M$, integrated over the whole length of the antenna and also over the radial thickness of the winding. Here N is the turns density per meter of length and M the turns density per meter of radial dimension. Thus, since $H = \sqrt{i\sigma/\omega\mu_0}\, E$, the effective length of the antenna is, in absolute magnitude,

$$\ell_e = \pi \frac{\sqrt{2}}{\delta} \int N M r^2 \, dz \, dr . \tag{B-1}$$

The resistance per turn is $2\pi r N M/\sigma_w$, which means that the total resistance is given by

$$R = \frac{2\pi}{\sigma_w} \int N^2 M^2 \cdot dz \, dr . \tag{B-2}$$

By applying the calculus of variations to (B.1) and (B.2), one can show that the minimum thermal ENF power spectrum, defined as $4 k_b T_k R/\ell_e^2$, is attained when N is a constant and M is proportional to r. Then the thermal ENF power spectrum $S_e(\omega)$ is given by

$$S_e(\omega) = \frac{8}{\pi} \cdot \frac{k_b T_k \delta^2}{\sigma_w b^4 \ell} \cdot \frac{1}{1 - (a/b)^4} \tag{B-3}$$

where k_b is Boltzmann's constant (1.38×10^{-23} J/deg.), T_k is the absolute temperature in degrees Kelvin, δ is the skin-depth in the ocean water, σ_w is the wire conductivity, 2ℓ is the total antenna length and b and a are the

outer and inner radii of the winding. (It is characteristic of all the various noise-source ENF's that they are independent of the turns density. Equation (B.3) exemplifies this fact for thermal ENF.)

To obtain a lower bound for the thermal ENF of the air-core antenna, it is convenient to assume that the total cable weight is assigned to the winding conductor. All the insulation, waterproofing jacket and other space within the cable are assumed to be of negligible weight. It is also assumed that these materials are infinitesimally thin where appropriate. Thus b is assumed to be the outside cable radius and the inner winding radius is chosen to make the cable density less than or equal to that of water. That is

$$
\frac{a}{b} = \begin{cases} (1 - 1/\rho_w)^{\frac{1}{2}}, & \rho_w > 1 \\ 0, & \rho_w \leq 1 \end{cases} \tag{B-4}
$$

where ρ_w is the relative density of the wire material.

Thus, from (B-3) and (B-4), if f = 45 Hz, σ = 4 mho/m, T_k = 300°K, 2ℓ = 300 m and b = 0.325 inches, then for an aluminum winding (ρ_w = 2.7, σ_w = 3.53 × 10^7 mho/m) the thermal ENF turns out to be -180.0 dBE. The lighter (but impractical) winding material sodium provides a 0.3 dB decrease in the ENF, while copper increases it by 2.2 dB.

APPENDIX C

SENSITIVITY DISTRIBUTION FOR ANTENNA WITH FERROUS CORE

If the H-field antenna has a ferromagnetic core, the magnetic flux in the core can be calculated only by solving an integral equation. Fortunately, however, interest here is confined to the total flux linkage rather than the flux linkage per unit length. The former is easily calculated (or measured) as shown below.

The transverse displacement of a towed antenna cable has been measured to be of the order of a micron (r.m.s. per root Herz). Thus the cable is essentially straight and so the effect of the flux in one element of the antenna core on another an arbitrary distance along the cable from it is described by the Green's function $G(z, z_o)$ of an ideally straight core.

Thus the small transverse displacement of the antenna causes a perturbation of the axial geomagnetic field component of amount $(B_y/\mu_o)\partial y/\partial z$ and a perturbation of the scattered magnetic field of $\int G(z, z_o) \Phi(z_o) dz_o$, where $\Phi(z)$ is the perturbation of the induced flux in the core. The total field perturbation H is the sum of these, and at the surface of the core it must be equal to Φ times the reluctance per unit length R of the core. That is

$$H(z) = \frac{B_y}{\mu_o} \frac{\partial y(z, t)}{\partial z} + \int G(z, z_o) \Phi(z_o) dz_o = R(z) \Phi(z) .$$

$$(C-1)$$

A second integral equation can be written for the different situation in which the incident field $N(z)I_o$ is provided by a current I_o in the

antenna winding of turn density $N(z)$.   Then

$$H_o(z) = N(z)I_o + \int G(z,z_o)\Phi_o(z_o)dz_o = R(z)\Phi_o(z) \qquad \text{(C-2)}$$

where the induced flux in the core is denoted by $\Phi_o(z)$ and the total field by $H_o(z)$.

Multiplying (C-2) by Φ and integrating over z, one obtains

$$I_o \int N(z)\Phi(z)dz + \int \Phi_o(z_o)\left[\int G(z_o,z)\Phi(z)dz\right]dz_o = \int R(z)\Phi_o(z)\Phi(z)dz, \qquad \text{(C-3)}$$

in which the symmetry of the Green's function (a consequence of the reciprocity theorem) has been invoked to reverse the order of the double integral. When the inner integral in (C-3) is replaced by the equivalent expression given by (C-1), the result is that two of the four integrals involved cancel, leaving

$$\int N(z)\Phi(z)dz = B_y \int \frac{\Phi_o(z)}{\mu_o I_o} \quad \frac{\partial y(z,t)}{\partial z} \quad dz .$$

But the left member is just the total change in flux linkage due to the transverse deformation of the antenna.   Its time derivative is therefore the motion-induced voltage, $v(t)$.   Hence

$$v(t) = B_y \int \frac{\Phi_o(z)}{\mu_o I_o} \cdot \frac{\partial^2 y(z,t)}{\partial z \partial t} \quad dz . \qquad \text{(C-4)}$$

Comparing (C-4) with (11), one sees that the equations are identical provided $A(z)N(z)$ of the air core case is now interpreted more generally as the ratio $\Phi_o(z)/\mu_o I_o$.   But if the length to diameter ratio of the core is large, this ratio is simply $\mu_a N(z)A(z)$, where μ_a is the relative permeability

of the core material. For a composite core, μ_a is the total flux within the winding divided by the external axial field strength and by the permeability of free space μ_o.

The "sensitivity profile" $\phi_o(z)/\mu_o I_o$ can also be directly measured by passing an alternating current I_o through the antenna winding and measuring the flux in the core from point to point by means of an external coaxial search coil.

APPENDIX D

CABLE MOTION DUE TO TURBULENT BOUNDARY LAYER STRESSES

There are perpendicular pressure fluctuations and tangential shear stress fluctuations on the cable surface associated with the turbulent boundary layer in the water around the cable. There may be additional forces on the cable arising from vibrations of the tow point and from turbulence induced by the wake of the towing ship, but their contribution to the vibration of the cable in the antenna region can, in principle, be made arbitrarily small by using a long enough tow line. Thus a lower bound on the vibration level of the cable is that generated by the locally-induced turbulent boundary layer around the cable. Its characteristics are determined only by the towing speed and the diameter of the cable. (Presumably, the surface can be made smooth enough that surface roughness is not a factor. Franz [13] gives as a criterion of hydraulic smoothness the condition that the height of the surface perturbations, in inches, shall be not greater than 0.01 divided by the towing speed in knots. Angle of incidence seems also not to be a factor since the transverse drag component is small compared with the longitudinal component at the tow-angles taken by this nearly neutrally-buoyant cable.)

It $p(\theta, z, t)$ represents the pressure on the cable surface as a function of position θ, z and time t, the transverse force per unit length, assuming the shear stresses are relatively insignificant, is

$$f(z, t) = a \int_{-\pi}^{\pi} p(\theta, z, t) \cos \theta \, d\theta .$$

The correlation function $C_f(\zeta, \tau)$ of the transverse force distribution is given therefore by

$$C_f(\zeta, \tau) = \langle f(z, t) f(z + \zeta, t + \tau) \rangle$$

$$= a^2 \int_{-\pi}^{\pi} \langle p(\theta, z, t) p(\theta', z + \zeta, t + \tau) \rangle \cos \theta \cos \theta' \, d\theta \, d\theta'$$

where the brackets $\langle \rangle$ denote expected value. If the transverse correlation distance is small compared with the circumference of the cylinder, the expected value in the integrand is non-negligible only when θ is close to θ'. In that case, therefore, $C_f(\zeta, \tau)$ can be written approximately as

$$C_f(\zeta, \tau) = a^2 \int_{-\pi}^{\pi} C_p(\psi, \zeta, \tau) \, d\psi \int_{-\pi}^{\pi} \cos^2 \theta \, d\theta$$

$$= \pi a^2 \int_{-\pi}^{\pi} C_p(\psi, \zeta, \tau) \, d\psi \tag{D-1}$$

Also implicit in this result is the assumption that the pressure fluctuations are statistically uniform in azimuth.

The two-dimensional spectral density $S_f(k, \omega)$ of the transverse force distribution is simply the double Fourier transform of $C_f(\zeta, \tau)$. That is,

$$S_f(k, \omega) = \int C_f(\zeta, \tau) e^{i\omega \tau - ik\zeta} \, d\tau \, d\zeta,$$

where the limits of integration are $-\infty$ to ∞, or, from (D-1)

$$S_f(k, \omega) = \pi a^2 \int d\tau \, d\zeta \int_{-\pi}^{\pi} C_p(\psi, \zeta, \tau) e^{i\omega\tau - ik\zeta} \, d\psi$$

$$= \pi a^2 \int_{-\pi}^{\pi} d\psi \int \widetilde{C}_p(\psi, \zeta, \omega) e^{-ik\zeta} \, d\zeta. \tag{D-2}$$

Here $\widetilde{C}_p(\psi, \zeta, \omega)$ is the cross-spectral density of the pressure fluctuations at two points separated in azimuth by ψ and axially by ζ, and given by

$$\widetilde{C}_p(\psi, \zeta, \omega) = \int C_p(\psi, \zeta, \tau) e^{i\omega\tau}\, d\tau \ .$$

It is, with ψ written as ξ/a, the function $\Gamma(\omega, \xi, \zeta)$ studied by Bakewell [14] on a truncated cylinder of large radius.

There appear to be no data available on the surface pressure fluctuations on small cylinders and so this derivation must continue on the assumption that Bakewell's data is applicable. The error incurred by such an assumption may be large, because Bakewell showed that his data were in very close agreement with data obtained on flat surfaces. The cable, however, has a radius of curvature which is certainly not large compared with the thickness of the boundary layer, and so cannot be regarded as flat.

However, proceeding formally, one can express $\widetilde{C}_p(\psi, \zeta, \omega)$ from Bakewell, for $-\pi \leq \psi \leq \pi$, as

$$\widetilde{C}_p(\psi, \zeta, \omega) = \varphi(\omega)\, A(\omega\zeta/U_c)\, B(\omega a \psi/U_c)\, e^{-i\omega\zeta/U_c} \qquad (D-3)$$

where U_c is the convection velocity at frequency ω. Bakewell measured the functions φ, A, B and U_c experimentally. He presents the results graphically, but it would appear that his $A(\chi)$ and $B(\xi)$ functions are well represented by the expressions $A(\chi) = \exp(-|\chi|/10)$ and $B(\xi) = \exp(-|\xi|)$. Substituting these expressions in (D-3) and then integrating, in the manner defined by (D-2) to obtain $S_f(k, \omega)$, one finds

$$S_f(k, \omega) \approx \frac{2\pi}{5}\, a\, \frac{U_c^2}{\omega^2}\, \varphi(\omega)\, \frac{1}{0.01 + (1 + kU_c/\omega)^2} \ . \qquad (D-4)$$

69

(The finite limits of integration in (D2) were extended to infinity to obtain this result. This approximation is consistent with the assumption that the transverse correlation distance is small compared with the circumference of the cylinder. The assumption is, in fact, only marginally justified for the correlation distance measured on flat surfaces. It seems reasonable to hypothesize, however, that on this more curved surface the correlation distance would be smaller.)

The corresponding spectrum $S_y(k,\omega)$ of the cable displacement is therefore (see Appendix E)

$$S_y(k,\omega) = \left| H_t(k,\omega) \right|^2 S_f(k,\omega) \tag{D-5}$$

where $H_t(k,\omega)$ is the transfer function for transverse displacement, and the spectrum $S_y(\omega)$ of the displacement of a particular point is

$$S_y(\omega) = \frac{1}{2\pi} \int \left| H_t(k,\omega) \right|^2 S_f(k,\omega)dk . \tag{D-6}$$

By examining the form taken by $H_t(k,\omega)$ (Appendix E) and $S_f(k,\omega)$ as defined by (D-4), one concludes that for a cable having properties similar to those of the existing buoyant cable (Appendix I), the peak in $S_f(k,\omega)$ occuring at $k = -\omega/U_c$ is far enough away from the region in which $\left| H_t(k,\omega) \right|^2$ has non-negligible magnitude, that it is sufficient to assume $S_f(k,\omega) \approx S_f(0,\omega)$ and take it outside the integral sign. Since $\left| H_t(k,\omega) \right|^2$ is symmetrical, its peaks at $\pm k_\ell$ pick up a contribution proportional to $[S_f(-k_\ell,\omega)+S_f(k_\ell,\omega)]/2$, which is close to being equal to $S_f(0,\omega)$ even though $S_f(-k_\ell,\omega) > S_f(0,\omega)$ and $S_f(k_\ell,\omega) < S_f(0,\omega)$. Therefore $S_y(\omega)$ can be written as

$$S_y(\omega) = S_f(0,\omega) \; \frac{k_t Q_t}{\pi \omega^4 |m_t|^2} \quad , \tag{D-7}$$

with k_t, Q_t and m_t defined in Appendix E.

The motion-induced ENF of the E-field antenna, for example, can be obtained immediately by combining (D-4) with (G-6). The result is, after some re-ordering,

$$S_e(\omega) = \frac{B_y^2}{5\pi(1+b)^2} \cdot \frac{\delta^*}{a} \cdot \frac{\varphi(\omega)}{\rho^2 U_\infty^3 \delta^*} \cdot \frac{U_c^2}{U_\infty^2} \cdot \frac{U_\infty^5}{\omega^4 \ell a^2}$$

$$\tag{D-8}$$

in which U_∞ is the towing speed and b is the buoyancy of the cable (its weight divided by the weight of the displaced water). The length δ^* is the displacement thickness of the boundary layer [15], and is the thickness within which most of the change in average water velocity between the cable surface and the water velocity at infinity has been accomplished. It will probably be some small part of a cable diameter. The water mass density is denoted by ρ.

The factors in (D-8) are arranged in order of increasing strength of variation. The first, involving B_y and b, is essentially a constant. The same is true for the second, except that its value is uncertain. The third and fourth, presented graphically by Bakewell [14], are of relatively slow variation, while the last is a very strong function of towing speed and frequency and a fairly strong function of radius and antenna length.

71

The U_∞^5 and ω^{-4} dependencies appear to correspond fairly well with the measured data. Figure 3 shows a 12.5 dB increase in ENF as the speed is increased from 8 to 14 knots, whereas $50 \log_{10}(14/8)$ is 12.2 dB, and the slope of the curves appears to follow the ω^{-4} law. The quantitative correspondence is not so good, however. Taking $B_y = 0.5$ gauss, $U_\infty = 14$ knots, $b = .75$, $\ell = 150$ m, $a = 0.325$ inches, $f = 45$ Hz and $\delta* = a/3$, one finds $f \delta*/U_\infty = 0.0172$, so that $\varphi(\omega)/(\rho^2 U_\infty^3 \delta*)$ is, from Bakewell [14], about -45 dB and U_c/U_∞ is 0.87. This leads to $S_c(\omega)$ being -189.1 dBE whereas the corresponding measured value (at 14 knots and 45 Hz) is, from Fig. 3, -205 dBE. Thus the estimate from turbulence theory is 16 dB too large. This may well be attributable directly to the fact that flat-surface pressure data is being used to make predictions about a strongly curved surface.

The derivation for longitudinal vibration excited by axially-directed shear stress fluctuations at the cable surface is essentially the same, with modified notation, except that the $\cos \theta$ factor in (D-1) does not appear. Thus the length/time correlation function $C_s(\zeta, \tau)$ of the axial force per unit length is given by

$$C_s(\zeta, \tau) = 2 \pi a^2 \int_{-\pi}^{\pi} C_\sigma(\psi, \zeta, \tau) \, d\psi \quad , \tag{D-9}$$

where $C_\sigma(\psi, \zeta, \tau)$ is the correlation function of the shear stress at points separated in azimuth by ψ, length by ζ and time by τ.

The double Fourier transform of $C_s(\zeta, \tau)$ gives the spectral density $S_s(k, \omega)$ of the axial force on unit length and so the spectral density

72

$S_x(k, \omega)$ of the longitudinal cable displacement is simply

$$S_x(\kappa, \omega) = \left| H_\ell(k, \omega) \right|^2 S_s(k, \omega) \qquad \text{(D-10)}$$

and, assuming that $S_s(k, \omega)$ is essentially equal to $S_s(0, \omega)$ over the range of k for which $\left| H_\ell(k, \omega) \right|^2$ has non-negligible magnitude, one finds

$$S_x(\omega) = \frac{k_\ell Q_\ell}{\pi \omega^4 \left| m_\ell \right|^2} S_s(0, \omega) \quad . \qquad \text{(D-11)}$$

APPENDIX E

CABLE DYNAMICS

For transverse vibration, the cable is a long beam with a certain bending stiffness EI, non-uniform tension $T(z)$ and effective mass (see Appendix F) per unit length m_t *excited* into transverse vibration by a transverse force distribution f. Its equation of motion is well known [12] to be

$$\left\{ EI \frac{\partial^4}{\partial z^4} - \frac{\partial}{\partial z} \left[T(z) \frac{\partial}{\partial z} \right] + m_t \frac{\partial^2}{\partial t^2} \right\} y(z, t) = f(z, t).$$

(E-1)

Energy dissipation will limit the cable perturbation caused by a single point force at $z = z_o$ to a finite region containing the point of application. If the tension is essentially uniform over this region, then the cable perturbation can be calculated accurately by assuming that the tension is truly uniform and has the value $T(z_o)$. Then (E-1) can be written

$$\left\{ EI \frac{\partial^4}{\partial z^4} - T(z_o) \frac{\partial^2}{\partial z^2} + m_t \frac{\partial^2}{\partial t^2} \right\} y_o(z, t) = f_o(t) \delta(z - z_o)$$

(E-2)

where $f_o(t)$ is the magnitude of the force and $\delta(z-z_o)$ is the Dirac delta function.

Taking the double Fourier transform of (E-2), one can rewrite it in the spatial and temporal frequency domain as follows:

$$\left(EI k^4 + T(z_o) k^2 - \omega^2 m_t \right) Y_o(k, \omega) = F_o(\omega) e^{-ikz_o}$$

Thus the spectral amplitude $Y_o(k, \omega)$ of the cable displacement is given by

$$Y_o(k, \omega) = H_t(k, \omega) F_o(\omega) e^{-ikz_o} \qquad \text{(E-3)}$$

where

$$H_t(k, \omega) = \frac{1}{EI\,k^4 + T(z_o)k^2 - \omega^2 m_t} \qquad \text{(E-4)}$$

and it is understood that $H_t(k, \omega)$ is also a function of z_o.

Since $G_o(z, \omega)$ and $H_t(k, \omega)$ are a transform pair in the $k \rightarrow z$ transformation, defined in equations (24), then $\int G_o(z, \omega)dz$ is simply $H_t(0, \omega)$ which, from (E-4) is just $-1/(\omega^2 m_t)$.

In a manner entirely paralleling that used in the temporal frequency domain to study the effect of linear filters on randomly time-varying input signals, one can show that the spectral density $S_y(k, \omega)$ in the spatial and temporal frequency domain of the transverse cable displacement $y(z, t)$ induced by the statistically uniform and stationary transverse force spectrum $S_f(k, \omega)$ is given by

$$S_y(k, \omega) = \left| H_t(k, \omega) \right|^2 S_f(k, \omega) \qquad \text{(E-6)}$$

The resulting spectral density $S_y(\omega)$, in the temporal frequency domain only, of the transverse displacement of a particular point on the cable is therefore given by

$$S_y(\omega) = \frac{1}{2\pi} \int S_y(k, \omega)\,dk \qquad \text{(E-7)}$$

or, by virtue of (E-6)

75

$$S_y(\omega) = \frac{1}{2\pi} \int \left| H_t(k,\omega) \right|^2 S_f(k,\omega)\, dk \qquad (E\text{-}8)$$

In the present application, $S_f(k,\omega)$ is essentially flat over the region in which $H_t(k,\omega)$ has non-negligible magnitude. Therefore (E-8) can be rewritten approximately as

$$S_y(\omega) \approx S_f(0,\omega) \frac{1}{2\pi} \int \left| H_t(k,\omega) \right|^2 dk . \qquad (E\text{-}9)$$

This, in turn, can be expressed in terms of the mechanical Q-factor for transverse vibration, defined as

$$Q_t = \frac{1}{2 k_t} \int \left| \frac{H_t(k,\omega)}{H_t(0,\omega)} \right|^2 dk , \qquad (E\text{-}10)$$

where k_t is the (real) value of k at which $H_t(k,\omega)$ is a maximum. Thus (E-9) becomes

$$S_y(\omega) \approx \frac{k_t Q_t}{\pi} \left| H_t(0,\omega) \right|^2 S_f(0,\omega) \qquad (E\text{-}11)$$

$$\approx \frac{k_t Q_t}{\pi \omega^4 |m_t|^2} S_f(0,\omega) . \qquad (E\text{-}12)$$

The peaks of $\left| H_t(k,\omega) \right|^2$ at $k = \pm k_t$ are associated with poles of the same function lying near the real axis at the complex values of k for which the denominator on the right in (E-4) has a zero. The zeros of the denominator are the four characteristic wave numbers $\pm k_1$, $\pm k_2$, given by

$$k_1 = \left\{ \left[\frac{\omega^2 m_t}{EI} + \left(\frac{T}{2\,EI} \right)^2 \right]^{\frac{1}{2}} - \frac{T}{2\,EI} \right\}^{\frac{1}{2}}$$

$$k_2 = i \left\{ \left[\frac{\omega^2 m_t}{EI} + \left(\frac{T}{2\,EI} \right)^2 \right]^{\frac{1}{2}} + \frac{T}{2\,EI} \right\}^{\frac{1}{2}} \qquad (E\text{-}13)$$

and, since the poles near the real axis are those at $\pm k_1$, the peaks of $|H_t(k,\omega)|^2$ occur at the values of k given accurately by

$$k_t = \text{Re}\{k_1\}. \qquad (E-14)$$

By substituting (E-4) into (E-10) and evaluating the integral by the calculus of residues, one finds the following explicit expression for Q_t

$$Q_t = -\frac{\pi}{2k_t}|k_1 k_2|^4 \text{Re}\left\{\frac{1}{k_1^2 - k_2^2}\left[\frac{1}{k_1 \text{Im}\{k_1^2\}(k_1^2 - k_2^{*2})}\right.\right.$$

$$\left.\left. -\frac{1}{k_2 \text{Im}\{k_2^2\}(k_2^2 - k_1^{*2})}\right]\right\} \qquad (E-15)$$

For longitudinal vibration, the theory is simplified considerably because the equation of motion is a second-order differential equation rather than a fourth-order one. It is, explicitly,

$$\left\{AE\frac{\partial^2}{\partial z^2} - m_\ell\frac{\partial^2}{\partial t^2}\right\} x(z,t) = -s(z,t) \qquad (E-16)$$

where AE is the stretching stiffness, m_ℓ the effective vibrating longitudinal mass per unit length, $x(z,t)$ the longitudinal displacement and $s(z,t)$ the longitudinal external force per unit length. There is no z-dependence of the coefficients in this equation, a further simplification.

In the two-dimensional transform space, the equation becomes

$$(AE k^2 - \omega^2 m_\ell) X(k,\omega) = S(k,\omega) \qquad (E-17)$$

so that the transfer function $H_\ell(k,\omega)$ relating longitudinal cable displacement to externally applied longitudinal force is given by

77

$$H_\ell(k,\omega) = \frac{1}{AEk^2 - \omega^2 m_\ell} \quad . \tag{E-18}$$

Thus if the applied longitudinal forces are statistically stationary and uniform, characterized by a spectral density $S_s(k,\omega)$, the spectral density $S_x(k,\omega)$ of the resulting cable displacement is given by

$$S_x(k,\omega) = \left| H_\ell(k,\omega) \right|^2 S_s(k,\omega) \tag{E-19}$$

and the spectral density $S_x(\omega)$ of the longitudinal displacement at a particular point is

$$S_x(\omega) = \frac{1}{2\pi} \int \left| H_\ell(k,\omega) \right|^2 S_s(k,\omega)\, dk \quad . \tag{E-20}$$

On the assumption that $S_s(k,\omega)$ is essentially flat over the region of the k-axis in which $H_\ell(k,\omega)$ has non-negligible magnitude, (E-20) can be rewritten as

$$S_x(\omega) \approx \frac{1}{2\pi} \int \left| H_\ell(k,\omega) \right|^2 dk\, S_s(0,\omega)$$

$$\approx \frac{k_\ell Q_\ell}{\pi} \left| H_\ell(0,\omega) \right|^2 S_s(0,\omega) \tag{E-21}$$

$$\approx \frac{k_\ell Q_\ell}{\pi \omega^4 \left| m_\ell \right|^2} S_s(0,\omega)$$

Here $\dot{Q}_\ell$ is the Q-factor for longitudinal cable vibrations, given by

$$Q_\ell = \frac{1}{2k_\ell} \int \left| \frac{H_\ell(k,\omega)}{H_\ell(0,\omega)} \right|^2 dk$$

$$= \frac{\pi \left| k_o \right|^2}{4 k_\ell \,\mathrm{Im}\{k_o\}} \tag{E-22}$$

in which $\pm k_o$ are the poles of the transfer function $H_\ell(k, \omega)$, given by

$$k_o = \omega \sqrt{\frac{m_\ell}{EA}} \qquad (E-23)$$

and $\pm k_\ell$ are the locations of the peaks of $\left| H_\ell(k, \omega) \right|^2$, given accurately by

$$k_\ell = Re\left\{k_o\right\} . \qquad (E-24)$$

APPENDIX F

EFFECTIVE VIBRATING MASS PER UNIT LENGTH

To derive the form of the effective vibrating mass per unit length, the classical (laminar) theory of small vibrations of immersed objects will be invoked [11].

If $\overline{u} = \hat{x}u$ is the transverse cable velocity (at radian frequency ω) and $\overline{v}$ is the water velocity, then everywhere but in the (laminar) boundary layer, $\overline{v}$ is the gradient of a potential and the normal component of $\overline{v} - \overline{u}$ must be zero at the cable surface. Thus in cylindrical coordinates

$$\psi(r, \theta) = -u \frac{a^2}{r} \cos \theta \qquad (F-1)$$

$$\overline{v}(r, \theta) = \nabla \psi = u \frac{a^2}{r^2} (\hat{r} \cos \theta + \hat{\theta} \sin \theta), \qquad (F-2)$$

where a is the cable radius.

The water pressure p is given by $\nabla p = i\omega \rho \overline{v}$, so that

$$p(r, \theta) = i\omega \rho \psi(r, \theta) \qquad (F-3)$$

Thus the perpendicular force per unit area on the cable surface is $-p(a, \theta)$ in the radial direction, and the tangential force per unit area on the cable surface is $[\overline{v}(a, \theta) - \overline{u}] \cdot \hat{\theta}(1 - i)\rho\sqrt{\omega\upsilon/2}$ in the azimuthal direction, since $[\overline{v}(a, \theta) - \overline{u}] \cdot \hat{\theta}$ is the difference in velocity across the boundary layer. Here ρ is the water mass density and υ the kinematic viscosity of the water.

The total x-directed drag force on the cable is therefore

$$f_d = \int_0^{2\pi} \left\{ -p(a, \theta) \cos \theta - [\overline{v}(a, \theta) - \overline{u}] \cdot \hat{\theta}(1 - i)\rho\sqrt{\omega\upsilon/2} \sin \theta \right\} a d\theta .$$

$$(F-4)$$

Substituting (F-1), (F-2) and (F-3) into (F-4) and carrying out the integration, one finds

$$f_d = -\pi a^2 \rho [1 + i(1-i)\delta_w/a](-i\omega u) \qquad (F-5)$$

where $\delta_w = \sqrt{2\upsilon/\omega}$ and is the skin depth for plane shear wave propagation in the water.

If the cable is being driven by a uniform transverse force distribution f and if m_c is the mass per unit length of the cable alone, then the total force is $f + f_d$ and by Newton's law

$$f + f_d = m_c(-i\omega u),$$

since $-i\omega u$ is the acceleration. From (F-5), this can be written

$$f = \{m_c + \pi a^2 \rho [1 + i(1-i)\delta_w/a]\}(-i\omega u),$$

which shows that the cable behaves as though it had an effective mass distribution m_t (for transverse vibration) given by

$$m_t = m_c + \pi a^2 \rho [1 + i(1-i)\delta_w/a)]$$

In practice, $\delta_w/a << 1$ and so this can be expressed simply as

$$m_t = m_c + \pi a^2 \rho (1 + i\delta_w/a) \qquad (F-6)$$

Thus the cable behaves in transverse vibration as though it had an effective mass equal to the cable mass plus the mass of the displaced water and, in addition, has a small imaginary mass equal to δ_w/a times the mass of the displaced water representing the viscous energy dissipation.

For longitudinal vibration, the surrounding water remains essentially stationary except in the boundary layer. Thus if $\hat{z}u$ is the

longitudinal cable velocity (at radian frequency ω) then the shear force per unit area in the z-direction on the cable surface is $-u(1-i)\rho\sqrt{\omega\upsilon/2}$. The total z-directed viscous force f_d per unit length of cable is therefore

$$f_d = -\pi a^2 \rho\, i(1-i)\, \delta_w\big/a\, (-i\omega u).$$

Following the same derivation as before, one finds that for longitudinal vibration the cable behaves as if it had a mass per unit length m_ℓ given by

$$m_\ell = m_c + \pi a^2 \rho\, (i\, \delta_w/a). \tag{F-7}$$

It should be noted that this derivation of both m_t and m_ℓ has been carried out using a laminar-flow model. Intuitively one might expect that the effect of the turbulence is merely to superimpose an additional velocity field that is moved bodily by the cable vibration. Since all displacements are small, the interaction between the turbulence and the vibration can be assumed to be negligible, allowing one to combine linearly the effects of each one acting alone. The adequacy of this interpretation is not in doubt for calculating the additional real part of the mass in the case of transverse vibration (see, for example, Wambsganss and Boers [18]). It remains a hypothesis, however, for the imaginary (damping) part.

APPENDIX G

MOTION-INDUCED ENF IN THE E-FIELD ANTENNA

The derivation of the motion-induced ENF in the E-field antenna follows very closely that carried out for the H-field antenna in Section IV. It is simpler, however, because the "profile roughness" component is not present.

In place of (11), the fundamental equation is

$$v(t) = B_y \int u(z) \frac{\partial x(z,t)}{\partial t} \, dz , \qquad (G-1)$$

which, in the frequency domain, becomes

$$V(\omega) = -i\omega B_y \int u(z) X(z,\omega) \, dz \qquad (G-2)$$

which has the same form as (14) except that $u(z)$ appears instead of $u'(z)$. In these equations, $u(z)$ is equal to 1 for $|z| < \ell$ and is zero otherwise and, with the geomagnetic field lying in the yz plane, only x-directed vibrations generate motion-induced noise.

By following the same derivation as before, but noting that the effective length is now $\int u(z) dz = 2\ell$, one finds the following expression for the equivalent noise field power spectral density $S_e(\omega)$

$$S_e(\omega) = \omega^2 B_y^2 \frac{1}{2\pi} \int \left| \frac{U(k)}{U(0)} \right|^2 \left| H_t(k,\omega) \right|^2 S_f(k,\omega) \, dk \qquad (G-3)$$

in which

$$U(k) = \int u(z) e^{-ikz} \, dz = 2\ell \frac{\sin k\ell}{k\ell} . \qquad (G-4)$$

As before, one assumes that $S_f(k,\omega)$ is essentially equal to $S_f(0,\omega)$ over the range of k for which the remainder of the integrand has non-negligible amplitude. Then, including the contribution of the peak in U(k) at k = 0 and that of the peaks in $|H_t(k,\omega)|$ at $\pm k_t$, one finds, approximately

$$S_e(\omega) = \frac{1}{2\ell} \left(\frac{B_y}{\omega |m_t|} \right)^2 S_f(0,\omega) \left\{ 1 + \frac{Q_t}{\pi k_t \ell} \right\} . \qquad \text{(G-5)}$$

It may be shown by leaving u(z) initially unspecified that the "long profile" motion-induced ENF of the E-field antenna is minimized by the profile u(z) which minimizes the functional $\int u^2(z)\,dz / [\int u(z)dz]^2$. The calculus of variations then enables one to verify that the minimizing profile is, in fact, the one already possessed by the E-field antenna, namely, u(z) = 1 for $|z| < \ell$ and zero otherwise.

The "shortness" correction term $Q_t / (\pi k_t \ell)$ in (G-5) is negligible for long E-field antennas, in which case the motion-induced ENF becomes simply

$$S_e(\omega) = \frac{1}{2\ell} \left(\frac{B_y}{\omega |m_t|} \right)^2 S_f(0,\omega) . \qquad \text{(G-6)}$$

This equation shows that the motion- nduced ENF is independent of any mechanical property of the antenna cable except for its diameter (m_t is essentially unavailable for modification once the cable diameter is fixed, since the cable will invariably be close to neutrally buoyant).

There is an additional noise generated by the electrodes of the E-field antenna [6]. It is now believed that motion-induced noise is the limiting noise for the long antennas of current interest, however.

APPENDIX H

EFFECT OF NON-UNIFORM CABLE TENSION

The express on for the motion-induced ENF of the H-field antenna, derived in Section IV and presented there as equation (33), has three terms. The first, the "long, smooth profile" contribution does not depend on the tension in the cable and therefore needs no modification. The second, the "shortness" contribution, arises from the discontinuity in the slope of the profile at each end of the antenna, as shown by equation (26) through (28) in Section IV. Since (33) was derived on the assumption of uniform tension, the "shortness" contribution is made up of two equal amounts, one from each end. The effect of non-uniform tension, therefore, is to make the contributions from each end of unequal magnitude. Thus $3 Q_t / (\pi k_t \ell)$ must be replaced by $3 \{ [Q_t(\ell)/k_t(\ell)] + [Q_t(-\ell)/k_t(-\ell)] \}/(2\pi \ell)$, since both Q_t and k_t depend upon the tension.

Finally, considering the "profile roughness" contribution, one notes that since this is generated over the whole length of the antenna, the tension-dependent terms must be averaged appropriately over the antenna length. This is accomplished by replacing the tension-dependent factor $k_t^3 Q_t S_\epsilon(k_t)$ by the average $\int u^2(z_0) k_t^3 Q_t S_\epsilon(k_t) dz_0 / \int u^2(z_0) dz_0$. The rationale for this is that the "profile roughness" contribution to the mean square noise voltage is proportional to the factors (i) $k_t^2 S_\epsilon(k_t)$ (because it is the <u>slope</u> of the profile roughness which is the important quantity), (ii) $u^2(z)$ (because, from (29), $\epsilon(z)$ is the fractional perturbation of the profile),

and (iii) $k_t Q_t$ (because, from (E-12), the local mean square displacement $S_y(\omega)$ is proportional to the tension-dependent quantity $k_t Q_t$ as well as to other tension-independent ones). In addition, the vibration at widely separated points is uncorrelated. Therefore, the total profile roughness contribution to the mean square motion-induced noise is proportional to the integral over the antenna length of the product of the factors i, ii and iii listed above.

The "shortness" correction term $Q_t / (\pi k_t \ell)$ for the E-field antenna, given in (G-5), also requires modification to include the effect of non-uniform tension. Since the term arises in the same way as that for the H-field antenna, namely from the profile discontinuity at each end, then the modification is effected in the same way. Thus the term becomes $[Q_t(\ell)/k_t(\ell) + Q_t(-\ell)/k_t(-\ell)] / (2\pi\ell)$. The "long, smooth profile" term (the "1" in (G-5)), requires no modification since it is tension-independent.

APPENDIX I

MECHANICAL PROPERTIES OF 0.65 INCH O.D. BUOYANT CABLE

To provide a quantitative context for the theory developed ι

the main text, the basic mechanical characteristics of the existing 0.65 O.D.

buoyant antenna cable are listed in this Appendix.

The particular cable specimen to which the following data apply

is that specified in Ref. [16]. It consists of a core of four 24 AWG insulated

copper conductors in a 0.165 inch O.D. polyethylene jacket surrounded by

a layer of 18 fiberglass strands to provide the necessary tensile strength

and jacketed overall by a 0.65 inch O.D. foamed polyethylene outer layer

to provide the necessary buoyancy.

Laboratory measurements at room temperature on a piece of

this cable indicate that the complex stiffness of the cable in bending (EI)

and stretching (EA) are essentially constant over the frequency band of

interest here (20 to 200 Hz) and have the values,

$$EI = 1.2(1 - i\,0.12) \text{ Newton m}^2 \qquad (I-1)$$

$$EA = 0.63 \times 10^6 \, (1 - i\,0.025) \text{ Newton.}$$

(If the tension is less than about 500 Newtons, the stretching stiffness is

less than this value, presumably due to slack strength members.) The

cable radius is 0.00825 m and its average relative density is 0.75, and

the mass density and viscosity of ocean water can be taken to be 10^3kg/m^3

and $10^{-6} \, \text{r}^2 \text{s}^{-1}$.

Using these values to calculate the wave number, mechanical Q-factor and attenuation for both transverse and longitudinal waves, one obtains the results presented in Figs. 8 through 11. The wave numbers and Q-factors are as defined by (E-14), (E-24), (E-15), (E-22) in conjunction with (E-13), (E-23), (F-6) and (F-7). The attenuations are defined by

$$\alpha_t = 20 \log_{10}(\exp[\text{Im}\{k_1\}])$$

$$\alpha_\ell = 20 \log_{10}(\exp[\text{Im}\{k_0\}]) .$$

(I-2)

Since the cable is uniform in its properties and has (presumably) no drogue at the far end, it has a uniform drag per unit length and uniform buoyancy per unit length. If the submarine maintains a constant depth, direction and speed therefore, the cable takes the form of a straight line and the tension increases linearly with distance from the free end. From Ref. [17] one can show that the angle θ (in radians) from the horizontal is given approximately by

$$\theta = \sqrt{\frac{\pi a (1-b)g}{1.1}} \; \frac{1}{U_\infty}$$

(I-3)

where b is the relative density of the cable and a its radius, g is the acceleration due to gravity and U_∞ is the towing speed. This can be expressed as

$$\theta^o \approx \frac{27}{U_{knot}}$$

(I-4)

where θ^o is the angle θ expressed in degrees and U_{knot} is the speed U_∞ expressed in knots.

Again, using Ref. [17], one can show that the tension T is given by

$$T = 0.02 \, a \, \rho U_\infty^2 d, \qquad\qquad (I-5)$$

where d is the distance from the free end.   This relationship is plotted
in Fig. 12.

REFERENCES

1. R. M. Bozorth, Ferromagnetism (Van Nostrand, New York, 1951).

2. J. R. Wait, Electromagnetic Waves in Stratified Media (Pergamon, New York, 1962), p. 22.

3. A. S. Griffiths, "ELF Noise Processing," Technical Report 490, Lincoln Laboratory, M. I. T. (13 January 1972), DDC AD-739907.

4. O. G. Nackoney, "Design of an ELF Loop Antenna Receiver," Technical Note 1972-22, Lincoln Laboratory, M. I. T. (11 July 1972), DDC AD-902159-L.

5. M. J. Lighthill, Fourier Analysis and Generalised Functions (Cambridge, London, 1960), p. 51 ff.

6. M. L. Burrows and C. W. Niessen "ELF Communication System Design" in Engineering in the Ocean Environment (Ocean 72) (IEEE, New York, 1972), pp. 95-109.

7. M. L. Burrows "Motion-Induced Noise in Tower Flexible Sensors" (24 March 1969), not generally available.

8. H. Bittel "Noise in Ferromagnetic Materials" IEEE Trans. MAG-5, No. 3, 359-365 (September 1969).

9. P. Mazzetti and G. Montalenti "Power Spectrum of the Barkhausen Noise of Various Magnetic Materials" J. Appl. Phys., Vol 34, No. 11, pp. 3223-3225 (November 1963).

10. J. E. Manning, "Vibration and Strain-Induced Noise from the ELF Flexible Loop Antenna," Technical Note 1971-51, Lincoln Laboratory, M. I. T. (15 December 1971), DDC AD-737093.

11. L. D. Landau and E. M. Lifschitz, Fluid Mechanics (Pergamon, London, 1959), Section 24.

12. E. Volterra and E. C. Zachmanoglou, _Dynamics of Vibrations_ (Merrill, Columbus, Ohio, 1965), Equations 4.5.2 and 4.5.86.

13. G. J. Franz, "Roughness Criteria and the Relationship Between Surface Roughness and Flow Noise," 75th Meeting of the Acoustical Society of America, Ottawa, 21-24 May 1968.

14. H. P. Bakewell, Jr., "Turbulent Wall-Pressure Fluctuations on a Body of Revolution," _J. Acoustical Society of America_, Vol. 43, No. 6, pp. 1358-63 (June 1968).

15. H. Tennekes and J. L. Lumley, _A First Course in Turbulence_ (M. I. T., Cambridge, 1972), pp. 191-2.

16. M. L. Burrows, "Fabrication of Flexible Loop Antenna," Technical Note 1970-31, Lincoln Laboratory, M. I. T. (5 October 1970), DDC AD-717718.

17. S. F. Hoerner, _Fluid Dynamic Drag_ (Published by the author, 1958), p. 3-11.

18. M. W. Wambsganss, Jr. and B. L. Boers, "Parallel-Flow-Induced Vibration of a Cylindrical Rod" Am. Soc. Mech. Eng. Winter Annual Meeting and Energy Systems Exposition, New York, N. Y., 1-5 December 1968.

19. R. L. Crane, "Motion Induced Noise in Flexible Electrode Pair and Loop Antennas" RCA David Sarnoff Research Center Technical Memo. No. 1 (July 1972).